Atmos. Chem. Phys. Discuss., 14, 377–434, 2014
www.atmos-chem-phys-discuss.net/14/377/2014/
doi:10.5194/acpd-14-377-2014


Atmospheric Chemistry and Physics Discussions



# Model study on the dependence of primary marine aerosol emission on the sea surface temperature

**S. Barthel, I. Tegen, R. Wolke, and M. van Pinxteren**

Leibniz Institute for Tropospheric Research, Permoser Straße 15, 04318 Leipzig, Germany

Received: 13 November 2013 – Accepted: 16 December 2013 – Published: 7 January 2014

Correspondence to: S. Barthel (barthel@tropos.de) and I. Tegen (tegen@tropos.de)

Published by Copernicus Publications on behalf of the European Geosciences Union.







## Abstract

Primary marine aerosol composed of sea salt and organic material is an important contributor to the global aerosol load. By comparing measurements from two EMEP (co-operative programme for monitoring and evaluation of the long-range transmissions of air-pollutants in Europe) intensive campaigns in June 2006 and January 2007 with results from an atmospheric transport model this work shows that accounting for the influence of the sea surface temperature on the emission of primary marine aerosol improves the model results towards the measurements in both months. Different sea surface temperature dependencies were evaluated. Using correction functions based on Sofiev et al. (2011) and Jaeglé et al. (2011) improves the model results for coarse mode particles. In contrast, for the fine mode aerosols no best correction function could be found. The model captures the low sodium concentrations at the marine station Virolahti II (Finland), which is influenced by air masses from the low salinity Baltic Sea, as well as the higher concentrations at Cabauw (Netherlands) and Auchencorth Moss (Scotland). These results indicate a shift towards smaller sizes with lower salinity for the emission of dry sea salt aerosols. Organic material was simulated as part of primary marine aerosol assuming an internal mixture with sea salt. A comparison of the model results for primary organic carbon with measurements by a Berner-impactor at Sao Vincente (Cape Verde) indicated that the model underpredicted the observed organic carbon concentration. This leads to the conclusion that the formation of secondary organic material needs to be included in the model to improve the agreement with the measurements.

## 1 Introduction

Sea salt dominates the aerosol mass in the marine atmosphere (O'Dowd and de Leeuw, 2007). Due to their high hygroscopicity sea salt aerosol (SSA) particles can be easily activated and act as cloud condensation nuclei (CCN) (Pruppacher and Klett,





ACPD
14, 377–434, 2014



1997; O'Dowd and Smith, 1993; Quinn et al., 1998; Murphy et al., 1998; Pierce and Adams, 2006). Sea salt droplets take part in heterogeneous chemical and microphysical transformations, thus influencing traces gases in the marine boundary layer (e.g., von Glasow et al., 2002). SSA also impacts the incoming radiation. In clear sky conditions it dominates the aerosol extinction of solar radiation over larger parts of the ocean, regionally contributing more than 75 % to the aerosol scattering (Haywood et al., 1999; Grini et al., 2002; Ma et al., 2008; Murphy et al., 1998). Its direct radiative effect is still highly uncertain (Lundgren et al., 2013), which is also reflected in the uncertainty in estimates of reduction of the radiation absorbed by the ocean between 0.08–6 $W m^{-2}$ (Lewis and Schwartz, 2004).

In addition to sea salt (SS), primary marine aerosol (PMA) can contain organic material (OM) (e.g, O'Dowd et al., 2004). The OM changes cloud condensation nuclei properties (Roelofs, 2008; Fuentes et al., 2010; Meskhidze et al., 2011; Westervelt et al., 2012), the direct and indirect radiative effects (Gantt et al., 2012a) and the aerosol chemistry (Smoydzin and von Glasow, 2007) compared to SS only.

Estimates of PMA distribution and effects are highly uncertain. A global source strength of 5000 $Tg yr^{-1}$ with a uncertainty factor of 4 has been reported by Lewis and Schwartz (2004). A comparison of different models showed global emission rates between 3 and 18 $Tg yr^{-1}$ (Textor et al., 2006). The high diversities in the modelled SS emission rates may be caused by insufficient process parameterisation of the emission in the currently available SS source functions. The main driver of PMA emission is the surface wind speed. While Ma et al. (2008) and Fan and Toon (2011) found no impact of the water temperature on the PMA emission fluxes, the parameterisations of Mårtensson et al. (2003), Jaeglé et al. (2011) and Sofiev et al. (2011) include the dependence on the sea surface temperature (SST). Jaeglé et al. (2011) and Sofiev et al. (2011) showed the importance of the temperature dependence for SS emission flux calculations at the global scale. At the regional scale this is indicated by the results of Tsyro et al. (2011). However, different measurements disagree in the resulting SST influence on PMA emission.





ACPD
14, 377–434, 2014



This study investigates the effect of SST-correction of the PMA emission flux for regional modelling. The correction functions for the PMA emission flux accounting for the SST by Jaeglé et al. (2011), Sofiev et al. (2011) and in addition a new parameterisation derived from Zábori et al. (2012) are compared with each other and with measurements from two intensive campaigns within the EMEP network in June 2006 and January 2007 as well as Berner-impactor measurements made at the Cape Verde Atmospheric Observatory at Sao Vincente in December 2007. The model simulations were carried out with the regional chemistry and aerosol transport model COSMO-MUSCAT (COnsortium of Small scale MOdelling – MUlti-Scale Chemical and Aerosol Transport model) for an "European" region including Iceland and an "African" region.

## 2 PMA emission processes

Two processes are mainly responsible for PMA emission. These are the tearing of drops from wave crests and the bursting of bubbles, which are formed by the entrainment of air to the ocean through breaking waves. The dislocation of water droplets from the wave crest occurs only at 10 m wind speeds above 7–11 $m\,s^{-1}$, producing the largest sea spray particles ("spume droplets" Monahan et al., 1983) with a minimum diameter of 40 µm and no defined maximum (Andreas, 1998). Such large droplets have high deposition and sedimentation velocities resulting in low residence times. Therefore they are less important for atmospheric microphysical and chemical processes and are usually neglected in large scale modelling.

The bubble bursting process is caused by bubbles rising back to the surface after the entrainment of air to the ocean. They emit two sorts of primary aerosols: small film droplets and larger jet droplets (Blanchard, 1963). Film droplets are formed during the collapse of a bubble from the water film, or cap of its top. During that process, up to a few hundred film droplets are produced per bubble. At 80 % relative humidity these droplets have typical radii of $r_{80} = 1\,\mu m$ and less (Lewis and Schwartz, 2004). Spiel (1998) found that film droplets are emitted mainly by bigger bubbles with a bubble ra-





ACPD
14, 377–434, 2014



dius $R > 2$ mm. The second type, the jet droplets are emitted from a vertical jet emerging from the bottom of the bubble. Up to 6–10 jet droplets per bubble (Mårtensson et al., 2003; Blanchard, 1983) are emitted by bubbles with radius $R < 3.4$ mm (Mårtensson et al., 2003). Their size distribution has its maximum around $r_{80} = 4\,\mu$m (O'Dowd and Smith, 1993).

The emission of PMA by bursting bubbles is influenced by parameters that control the bubble number and size distribution as well as parameters influencing the wave breaking activity. This includes the entrainment depth, SST, salinity or generally the composition of the water regarding OM or rather surfactants in the surface water. Wave breaking activity is controlled by the surface wind speed, wind fetch, wave height or the ocean bottom conditions (Lewis and Schwartz, 2004, and citations therein).

### 2.1 Wind speed dependence

Surface wind speed (10 m) is the only parameter controlling the emission rate in most of the SSA emission functions (Monahan et al., 1986; Smith et al., 1993; Smith and Harrison, 1998; Gong, 2003; Clarke et al., 2006). Wind stress at the ocean surface causes wave formation and wave breaking, leading to the entrainment of air and the production of bubbles in the ocean, but also causes the tearing of droplets from wave crests. Its impact on wave height and thus surface roughness length influences the vertical transport of aerosols by turbulence and thereby controlling the effective PMA production. The PMA production through bubble bursting has been found to be dependent on the particle production per whitecap area and the whitecap coverage, which were assumed to be independent from each other by Monahan et al. (1986) and Mårtensson et al. (2003), who treated only the whitecap coverage to be dependent on the wind speed. Mårtensson et al. (2003) found that the function $F \propto U_{10}^{3.41}$ of Monahan and O'Muircheartaigh (1980) for the whitecap coverage resulted in the most similar slope to the measurements by Nilsson et al. (2001), compared to others. Here, $F$ stands for the particle flux and $U_{10}$ for the wind speed at a height of 10 m. Keene et al. (2007) found the production of marine aerosol through bubble bursting to be proportional to





ACPD
14, 377–434, 2014



the amount of air detrained from the water column. With the assumption that all air, which entrains into the water column detrains as bubbles, the dependency $F \propto U_{10}^{3.74}$ was found (Long et al., 2011). This exponent is nearly the same as found by Wu (1979) for the whitecap dependency on surface wind speed.

## 2.2 Enrichment with organic material

OM can be an important part of PMA (e.g., Blanchard, 1964). Current parameterisations (Gantt et al., 2012b, and citations therein) afford a quantification of the amount of organics in the aerosols. Although many components and chemical species could be found, a large fraction is still unknown (e.g. Gantt and Meskhidze, 2013). This leads to considerable model uncertainties by using OM as universal tracer (Roelofs, 2008; Fuentes et al., 2010; Meskhidze et al., 2011; Westervelt et al., 2012; Gantt et al., 2012a). The fraction of OM in the PMA is found to be proportional to the primary production near the oceanic surface traced by the chlorophyll *a* concentration (O'Dowd et al., 2004; Sciare et al., 2009) and inversely proportional to the aerosol diameter (Barker and Zeitlin, 1972; Hoffmann and Duce, 1977; Oppo et al., 1999; O'Dowd et al., 2004; Rinaldi et al., 2009). The surface wind speed can further influence the organic to SS mass ratios in PMA (Gantt et al., 2011, and citations therein). The organic fraction in the oceanic surface water increases towards the surface (e.g. Russel et al., 2010) and forms surface films (Hardy, 1982) including surface-active material (Duce and Hoffmann, 1976). These surface films exist only under calm wind conditions and break up at 10 m wind speeds above $8\,m\,s^{-1}$ (Carlson, 1983). They can lead to wave suppression (Sellegri et al., 2006) resulting in lower emission rates. At higher wind speeds the concentration of organics in PMA is lower due to decreased near-surface concentration through stronger oceanic mixing. The surface active material surrounds the air bubbles in the water thus decreasing the gas exchange rate between the bubble and the water and increasing the rising speed of the bubbles (Lewis and Schwartz, 2004), resulting in changes in the bubble size spectra. Furthermore it stabilises the bubbles at





ACPD
14, 377–434, 2014



the ocean surface and allows them to thin out before bursting, which results in a shift of the particle spectra towards smaller sizes (Sellegri et al., 2006; Modini et al., 2013).

Summarising different measurements, Gantt and Meskhidze (2013) concluded that OM can displace SS or act as additional material in the emitted aerosols. This contribution is size dependend (Gantt and Meskhidze, 2013). Due to the lack of knowledge of a detailed quantification of that effect, it was decided to treat PMA as internal mixture with SS being replaced by OM for this work. With this assumption the volume of the total emitted PMA $V_P$ is is represented by:

$$V_P = V_{SS} + V_{OM}, \quad (1)$$

where $V_{SS}$ and $V_{OM}$ stands for the volumes of dry SS and OM respectively. The volume ratio $R_V$ between OM and SS is expressed as:

$$R_V = \frac{V_{OM}}{V_{SS}} \quad (2)$$

and the ratio $R_{Vp}$ between OM and dry PMA:

$$R_{Vp} = \frac{V_{OM}}{V_P}. \quad (3)$$

### 2.3 Dependence of PMA emission on SST

The SST can influence the physical processes controlling the PMA emission flux through bubble bursting via the viscosity of the water, the surface tension at the boundary between water and air, the molecular diffusivity and the solubility of gases. These properties impact on the coalescence of the bubbles, the gas exchange between the bubble and the surrounding water and the rising speed and thus the residence time of a bubble.

The kinematic viscosity of water decreases by a factor 2.2 with a temperature change from 0 to 30°C (e.g., Chen et al., 1973). This leads to a 2.2 times lower rise speed of





ACPD
14, 377–434, 2014



air bubbles at 0 °C due to the inverse proportional relationship assuming Stokes motion (Lewis and Schwartz, 2004). The resulting higher residence time in cold waters leads to an increase in the coalescence of bubbles, thus decreasing the number of smaller bubbles and increasing the number of bigger bubbles (Pounder, 1986).

The higher solubility of gases at cold temperatures in combination with the higher residence time of the bubbles lead to higher gas exchange rates between the bubble and the surrounding water. This is partly compensated by the lower diffusivity (Thrope et al., 1992). The gas exchange leads to a shrinking of the bubbles during their rise to the ocean surface. Smaller bubbles dissolve completely while bigger bubbles can survive. Higher exchange rates in colder waters lead to a decrease in the number of smaller bubbles resulting in a shift of the bubble size distribution towards bigger bubbles (see also Sect. 4.4.2., Fig. 35 Lewis and Schwartz, 2004).

Surface tension decreases only by 6 % for temperature changes between 0 and 30 °C, but may also impact the PMA emission. It may influence the breakup of bubbles in the water, bubble shape and the rising velocity as well as the breakup processes at the surface (Blanchard, 1963; Lewis and Schwartz, 2004).

In summary, lower SST lead to a decrease in the number concentration of small and an increase of large bubbles, resulting in a shift in the PMA size distribution.

Several laboratory studies confirm the influence of the SST on PMA emission (Bowyer et al., 1990; Mårtensson et al., 2003; Sellegri et al., 2006; Hultin et al., 2011; Zábori et al., 2012). Disagreements in the studies may be due to differences in the experimental setup. All authors found an increase in the number concentrations of small particles with decreasing temperature. Zábori et al. (2012) found a up to 10-fold increase for particles with diameter between 0.012 µm and 1.8 µm when reducing temperatures from 13–16 °C to 0 °C. Similarly Hultin et al. (2011) and Bowyer et al. (1990) also found a 4 to 5 times increasing particle number concentration with decreasing temperature for particles with a dry diameter of 0.02 µm to 1.8 µm and 0.25 µm to 1.5 µm respectively. Finally, Mårtensson et al. (2003) also found an increase up to a size of 0.1 µm in dry diameter with a continuous increase of the factor with decreasing particle





ACPD
14, 377–434, 2014



size. In contrast Zábori et al. (2012) found a local maximum factor between 0.18 µm and 0.57 µm at the maximum of the measured size distributions.

For particles bigger than 1.8 µm Zábori et al. (2012) observed constant number concentrations. In contrast, Bowyer et al. (1990) found a decrease by factor 2–3 for particles bigger than 1.5 µm with decreasing temperature. Sofiev et al. (2011) extrapolated the data of Mårtensson et al. (2003), which only included particles smaller than 2.8 µm, to larger particles and derived a factor of 4.5 for 2 µm and 10.5 for 10 µm between 5 and 15 °C.

While Mårtensson et al. (2003) found the number concentration of all particle sizes changed for all measured water temperatures, Zábori et al. (2012) found it to be constant above 10 °C. Hultin et al. (2011) and Bowyer et al. (1990) also found a constant number concentration above 14–15 °C for particles with dry diameter 0.02–2.8 µm and 0.25 to 2.5 µm, respectively.

### 2.3.1 Parameterisation of the SST correction factor

Two parameterisations of the temperature dependence of the PMA emission are currently available by Jaeglé et al. (2011) and Sofiev et al. (2011). Jaeglé et al. (2011) (thereafter named J11) compared measurements, which were made during six cruises conducted by NOAA's Pacific Marine Environmental Laboratory with model results. They found a strong relationship between the ratio of measured to modelled SSA-concentration and the SST. The model underestimated the measured ratios over water with a SST $T_W > 25$ °C and overestimated them over water with a SST $T_W < 10$ °C. With a third-order polynomial fit of the ratio between observation and model results they developed a correction function $c_J$ for the temperature dependence of the SSA emission fluxes $F(T_W) = c(T_W) F_0$, where $F_0$ is the uncorrected emission flux:

$$c_J(T_W) = 0.3 + 0.1 \cdot T_W - 0.0076 \cdot T_W + 0.00021 \cdot T_W, \quad (4)$$

with $T_W$ in °C. $c_J$ is independent of particle size and shifts from reducing to raising the emission rates at a water temperature around 21 °C. The second parameterisation by





ACPD
14, 377–434, 2014



Sofiev et al. (2011) (S11) was derived from the laboratory measurements of Mårtensson et al. (2003). Assuming the SSA flux needs no correction at the temperature of 25 °C the measured fluxes at $T_W$ = 15 °C, 5 °C and −2 °C were divided by $F$(25 °C). The resulting data were fitted by power law functions:

$$c_S(T_W, D_p) = a(T_W) \cdot D_p^{b(T_W)}, \quad (5)$$

where $D_p$ stands for the dry particle diameter and the parameters $a$ and $b$ are given in Table 1.

For SST other than in Table 1 the values for $c_S$ are derived by linear interpolation. This parameterisation is derived for the size range of 0.02 to 6–7 µm but applied to the size range of 0.01 to 10 µm in the model, which leads to uncertainties in the emission fluxes (Sofiev et al., 2011).

Since the shape of the size distribution for smaller particles differs strongly from the results by Zábori et al. (2012) a further parameterisation based on that data was tested, using the setup with 35‰ salinity and no surfactants. In those experiments the water temperature was slowly increased resulting in differing PMA size distributions. These size distributions were fitted with five lognormal distributions, which are used to generate the SST-correction function. Only the 0 °C- and the 13–16 °C-distributions are used by dividing them through each other similar to the method of Sofiev et al. (2011). It is assumed that the original PMA emission flux parameterisations are valid at the higher temperature. This result can be fitted by a further lognormal distribution for the factor $c_{Zb}$:

$$c_{Zb}(0\,^\circ\mathrm{C}, D_p) = \frac{\mathrm{d}c_0}{\mathrm{d}D_p} = \frac{4.492}{\sqrt{2\cdot\Pi}\cdot D_p \cdot 0.471} \cdot \exp\left[-0.5 \cdot \left(\frac{\log_{10} D_p - \log_{10} 0.44}{0.471}\right)^2\right] \quad (6)$$

or

$$c_{Zb}(0\,^\circ\mathrm{C}, D_p) = \frac{\mathrm{d}c_0}{\mathrm{d}\log D_p} = \frac{18.386}{\sqrt{2\cdot\Pi}\cdot 0.471} \cdot \exp\left[-0.5 \cdot \left(\frac{\log_{10} D_p - \log_{10} 0.136}{0.471}\right)^2\right], \quad (7)$$





ACPD
14, 377–434, 2014



where $c_0$ is the ratio between 0 °C and the 13–16 °C-distribution. Because of the low relative humidity in these experiments of 21–29 % and the deliquescence point of SS at 40 %, $D_p$ is taken to be the dry particle diameter in µm.

To take the temperature dependence into account, an interpolation between the value given by these equations at 0 °C and $c_{Zb}(13\,^{\circ}C, D_p) = 1$ was carried out. An exponential fit was selected, because the other two size distributions of Zábori et al. (2012) in the temperature ranges of 1–4 °C and 8–11 °C were reproduced at 2.6 °C and 12.2 °C better than with a linear fit (5.7 °C and 12.8 °C). Other fits were not possible due to insufficient data. Since Zábori et al. (2012) found no further influence for temperatures above 10 °C (8–14 °C depending on experimental setup) $c_{Zb}$ is set to 1 for all temperatures above 13 °C. This function based on Zábori et al. (2012) is further denoted as Zb13. The different correction functions are compared in Fig. 1.

## 3 Methods

### 3.1 Emission parameterisation

There is a wide variety of different parameterisations of SSA or PMA emissions (e.g. de Leeuw et al., 2011). The SS source function by Monahan et al. (1986) is known to provide good results in the bubble-derived size range (e.g., Andreas, 1998) except for particles smaller than 0.5 µm in dry diameter (Schulz et al., 2004). Newer parameterisations are normally evaluated against that source function (Gong, 2003; Mårtensson et al., 2003; Clarke et al., 2006; Long et al., 2011; Sofiev et al., 2011), or it is part of an emission function (e.g. Lundgren et al., 2013, which uses Mårtensson et al., 2003; Monahan et al., 1986; Smith et al., 1993). A comparison of the volume emission flux of four different source functions in Fig. 2 shows comparable results in the mid-size range. However, they differ strongly for the small and the large particles. During laboratory experiments it could be shown that particles as small as 10 nm can be produced by bubble bursting (Mårtensson et al., 2003; Sellegri et al., 2006). The four source





ACPD
14, 377–434, 2014



functions differ from each other in total number and shape of the size distribution for particles smaller than 100 nm. The highest emission rates are found for Long et al. (2011) and the smallest for Gong (2003) parameterization in that size range.

The Long et al. (2011)-parameterisation retrieved the best results in the comparison to measurements with a Berner-impactor at Sao Vincente (Cape Verde), and was chosen as basic emission function in this work. This source function uses a 2 mode approach for the description of the size distribution:

$$\frac{\mathrm{d}f_{\mathrm{Num}}}{\mathrm{d}\log_{10} D_{\mathrm{p80}}} = F_{\mathrm{Ent}} \cdot 10^{P_N} \tag{8}$$

where $F_{\mathrm{Ent}}$ is the term for the wind speed dependence (below), $f_{\mathrm{Num}}$ the particle number flux in $\mathrm{m^{-2}\,s^{-1}}$, $D_{\mathrm{p80}}$ the particle diameter at 80 % relative humidity in µm and $P_N$ is represented by the two modes, separated at 1 µm:

$$\begin{aligned} P_1 &= 1.46 \cdot (\log_{10}(D_{\mathrm{p80}}))^3 + 1.33 \cdot (\log_{10}(D_{\mathrm{p80}}))^2 - 1.82 \cdot (\log_{10}(D_{\mathrm{p80}})) + 8.83 \\ &\quad \text{for } D_{\mathrm{p80}} < 1\,\mu\mathrm{m} \\ P_2 &= -1.53 \cdot (\log_{10}(D_{\mathrm{p80}}))^3 - 8.1 \cdot (\log_{10}(D_{\mathrm{p80}}))^2 - 4.26 \cdot (\log_{10}(D_{\mathrm{p80}})) + 8.84 \\ &\quad \text{for } D_{\mathrm{p80}} > 1\,\mu\mathrm{m} \end{aligned} \tag{9}$$

Long et al. (2011) parameterized the wind speed influence on the particle production with the entrainment of air into the water column:

$$F_{\mathrm{Ent}} = 2 \times 10^{-8} \cdot U_{10}^{3.74} \tag{10}$$

For mixed PMA, Long et al. (2011) calculated the pure SS part of a particle size to determine emission rates. Since PMA is treated here as internal mixture without influence of the OM on the emission rates, we assume the total particle size to be composed of both SS and OM.

The dry SSA production depends on the salinity of the ocean water, which has to be considered while calculating the emission fluxes. The emission function of Long et al.





ACPD
14, 377–434, 2014



(2011) is based on the measurements of Keene et al. (2007) and Faccini et al. (2008). Keene et al. (2007) used sea water from the Bermuda Islands and Faccini et al. (2008) sampled aerosols 400 km off the Irish west coast. So in summary the salinity is approximately 35 ‰. To use this emission function for other salinities a corresponding particle size has to be calculated. It is assumed that the particle size is independent of salinity in the moment of the formation (RH = 98 %). With that assumption the source function defines the emission flux and the salinity the corresponding dry particle size. This will lead to a shift of the emitted particle size distributions towards smaller diameters for lower salinities, as reported by Zábori et al. (2012). No further influence of the salinity on the number production or size distribution (Mårtensson et al., 2003; Sofiev et al., 2011) has been taken into account.

The PMA emission schemes account for the fluxes at the measurement height, which is a few centimetres in case of laboratory bubble bursting experiments (Monahan et al., 1986; Bowyer et al., 1990; Mårtensson et al., 2003; Sellegri et al., 2006; Long et al., 2011) or a few meters in oceanic field studies (Smith et al., 1993; Smith and Harrison, 1998; Clarke et al., 2006). Therefore it is difficult to compare the source functions with each other because large particles quickly settle after emission. Thus the effective fluxes are calculated at a defined height. For this an equation by Hoppel et al. (2005) can be used:

$$\frac{F(z_2)}{F(z_1)} = \left(\frac{z_2}{z_1}\right)^{-\left(\frac{v_s}{\kappa \cdot u_*}\right)} \tag{11}$$

where $F$ is the PMA flux at the heights $z_1$ and $z_2$, $v_s$ the sedimentation velocity of the particle at 80 % relative humidity, $\kappa$ the von Kaarman constant and $u_*$ the friction velocity. For the height correction of surface fluxes we set $z_1 = z_0$, where $z_0$ is the surface roughness length. $z_0$ and $u_*$ are taken from the meteorological driver model COSMO (see below). Due to the gravitational losses only particles reaching the half level height of the lowest level ($z_{1/2}$) are taken into account, thus $z_2 = z_{1/2}$ (Fan and Toon, 2011).





ACPD
14, 377–434, 2014



To calculate the organic mass emitted with SS few parameterisations are available, which are summarised in a comparison study by Gantt et al. (2012b). Here the parameterisation by Long et al. (2011) is used together with the assumption that OM replaces SS in the emitted aerosols. For the calculation of the volume ratio $R_V$ of OM to dry SS (compare Eq. 2) Long et al. (2011) used the two-mode approach that was mentioned above:

For $D_{p80} < 1\,\mu m$:

$$R_{V,1}(D_{p80}, \text{chl } a) = 0.306 \cdot D_{p80}^{\delta_1} \tag{12}$$

with

$$\delta_1 = \frac{-2.01 \cdot 40 \cdot [\text{chl } a]}{1 + 40 \cdot [\text{chl } a]} \tag{13}$$

and for $D_{p80} > 1\,\mu m$:

$$R_{V,2}(D_{p80}, \text{chl } a) = \frac{0.056 \cdot 20.8 \cdot [\text{chl } a]}{1 + 29.8 \cdot [\text{chl } a]}. \tag{14}$$

The variables $D_{p80}$ and chl *a* represent the particle size at 80 % relative humidity in µm and the chlorophyll *a* concentration at the ocean surface in $\mu g\,L^{-1}$.

### 3.2 COSMO-MUSCAT

For this study the multi scale model system COSMO-MUSCAT (Wolke et al., 2012) is used. It was developed for process studies and operational forecast of pollutants and has been used in several air quality studies (Renner and Wolke, 2010) as well as large scale-transport studies of Saharan dust (Heinold et al., 2011). It is a online coupled system of COSMO developed by the German Weather Service (DWD) (Schättler et al., 2008) and MUSCAT (Wolke et al., 2012). The small-scale weather model COSMO is





ACPD
14, 377–434, 2014



the operational weather forecast model at DWD. It is used as driver for the meteorological input fields. For the initialisation and the boundary data of COSMO, the model simulations within this work used reanalysis data from GME (Global Model Earth) of the DWD, which were updated every three model hours. The chemistry-transport model MUSCAT treats aerosol and gas phase transport processes and chemical transformations. The transport processes in the model include advection, turbulent diffusion, sedimentation and size dependent dry and wet deposition as well as chemical and microphysical transformations (not regarded in this work) (Wolke et al., 2012). The aerosol size distribution is described with a mass based approach. This approach was extended for PMA to a spectral distribution using 15 logarithmically spaced bins which spread over the size range for the dry diameter from 0.01 to 10 µm. This number of bins has been chosen to optimize accuracy at reasonable computing times.

PMA emission fluxes are calculated using the parameterisation of Long et al. (2011) (Eqs. 9 and 10) assuming an internal mixture of OM and SS. The ratio of OM and SS at each size bin is also taken from Long et al. (2011) (Eqs. 12–14). The correction for the effective flux is described by Eq. (11). The salinity dependence of PMA emissions was accounted for through the calculation of the corresponding particle size at formation for both, the emitted particle at the actual salinity and the source function, where salinity is assumed at 35‰.

The removal processes are described by dry and wet deposition. For the dry deposition, the resistance approach is used (Seinfeld and Pandis, 2006), that accounts for atmospheric turbulence, aerodynamic and quasi-laminar layer resistance and gravitational settling. Dry deposition velocities are size dependent and calculated for every bin. Therefore the size bins are represented by the geometric mean radius with the addition of water according to Eq. (15) (below). Wet deposition is distinguished into washout, which describes the uptake of gases and particles by falling hydrometeors below clouds, and rainout, which accounts for the absorption of gases and particles by droplets within the clouds. For both types of wet removal processes the size dependent collection and scavenging efficiencies are used (Tsyro and Erdman, 2000).





ACPD
14, 377–434, 2014



### 3.3 Hygroscopic growth

The aerosols are treated as dry particles in the model. But since SS is hygroscopic and can growth up to four times larger in saturated air compared to the dry size (Monahan et al., 1986), wet particle sizes must be used for the calculation of the transport processes. For the calculation of the wet size of PMA the addition of water should be done accounting for both, SS and OM. The knowledge about the composition of OM is still incomplete (Gantt and Meskhidze, 2013). It has been found that it can be either hydrophilic or hydrophobic (Maria et al., 2004). Here, the influence of OM on water uptake is neglected resulting in the water uptake of the aerosols occurring only due to the SS. For the calculation of the growth of SSA we use the volume form of an equation by Lewis and Schwartz (2006):

$$\frac{V_{\text{wet}}}{V_{\text{dry}}} = \left(\frac{4}{3.7}\right)^3 \cdot \frac{2 - \text{RH}}{1 - \text{RH}}, \tag{15}$$

where RH is the relative humidity. Thus the water uptake by the aerosols is a diagnostic variable in the model, calculated at every time step.

Since the model transports aerosol masses, the densities are taken as 2165 kg m$^{-3}$ for SS (Keene et al., 2007), 1300 kg m$^{-3}$ for the OM and 1000 kg m$^{-3}$ for water.

### 3.4 Observational data

The model results from this work are compared to measurements from the EMEP monitoring network during the two intensive measurement campaigns in June 2006 and January 2007. The stations Birkenes (NO), Melpitz (GER), Virolahti (FI) (Tsyro et al., 2011; Yttri et al., 2008) as well as Auchencorth Moss (GB) and Cabauw (NL) representing different locations have been chosen for the comparison (Table 2). Auchencorth Moss near the east coast of Scotland has strong marine influence mainly from the Atlantic. During western winds some of the marine aerosol particles are deposited on the island, comparably to the stations Cabauw in the Netherlands and Birkenes in





ACPD
14, 377–434, 2014



southeast Norway. They are strongly influenced by marine air but located inland. Some particles can be removed before the air reaches the measurement sites. A further marine station is Virolahti II in southeast Finland, which is influenced by PMA from the low salinity Baltic Sea. The continental station Melpitz (Germany) represents long-range transport of PMA and is strongly impacted by deposition. These stations are equipped with filter pack, high- and low volume samplers and/or MARGA (Monitor for Aerosols and Gases in ambient Air) with additional chemical analysis at a height of 2 m. Mass concentrations for $PM_1$, $PM_{2.5}$ and $PM_{10}$ are determined daily. To trace SS the sodium concentration within the observed aerosol is used, which has only minor anthropogenic sources (Tsyro et al., 2011). For the conversion from SS to sodium mass a factor of 0.3061 is used (Seinfeld and Pandis, 2006).

While the EMEP stations represent the mid latitudes with lower SST, the measurements from the Cape Verde Atmospheric Observatory (CVAO) at Sao Vincente (Table 2) represent a region with higher SST. This island lays within the Cape Verde archipelago 700 km west of Africa. Its aerosol composition is dominated by mineral dust from the Sahara, biomass burning aerosol and aerosols of marine origin (Heinold et al., 2011; Müller et al., 2010, 2011). The measurements used here were obtained with a 5-stage Berner-impactor mounted at the top of a 30 m high tower 70 m inland off the coast to avoid direct influence by sea spray. The stages of this impactor were separated into: stage 1: 0.05–0.14 µm, stage 2: 0.14–0.45 µm, stage 3: 0.45–1.2 µm, stage 4: 1.2–3.5 µm, stage 5: 3.5–10 µm (Müller et al., 2010). The measurements used here have a daily frequency and were obtained in December 2007.

### 3.5 Description of case study and model setup

Three model simulations were carried out to capture all three measurement periods. For the comparison with the EMEP-stations in June 2006 and January 2007 an European region (Fig. 3) including the north east Atlantic as potential source for PMA was chosen. The model uses a horizontal grid resolution of 0.25° and 30 vertical model





ACPD
14, 377–434, 2014



layers in MUSCAT and 40 layers in COSMO. The mid-height of the lowest level is at approximately 10 m. The spin up time of the model is five days.

For the comparison to the measurements at Sao Vincente in December 2007 a second model domain is used (African domain) (Fig. 4). The grid resolution is the same as for the European domain except that $z_{1/2}$ = 33 m, which is close to the measurement height of the tower.

Further input data needed for the simulation of PMA emission are visualised in Figs. 3 and 4. Ocean surface salinity distribution is shown in Fig. 3 for the "European" domain. There, the yearly averaged values from the World Ocean Atlas 2001 at 0.25° grid resolution are taken.

The simulation of the fraction of OM within PMA requires the sea surface chlorophyll *a* concentration fields. Satellite retrievals provide the best spatial coverage. The chlorophyll product from MODIS-Aqua and MODIS-Terra were taken from the Ocean-Colour webpage. Here, the averages of the monthly mean values of both satellites were used. Missing data points were filled with the climatological monthly mean values. Remaining gaps were filled by linear interpolation (Fig. 4).

To take the influence of the SST on the PMA emission fluxes into account, SST data fields are needed. These were taken from COSMO based on the reanalysed input data of the GME model.

## 4 Model results

Since the emission flux and the vertical transport of PMA by turbulence are very sensitive to the surface wind speed it is important that the model reproduces this parameter realistically. Modelled surface wind speeds were compared to measurements made during the northward-directed Atlantic transec cruise number ANT-XXVII/4 of the research vessel *Polarstern*. The measurements of the wind speed at the *Polarstern* were made at 37 m-height, which is approximately the half level height of the lowest level of the "African" domain. The model first layer wind speeds are plotted against these





ACPD
14, 377–434, 2014



observations in Fig. 5. The model slightly underestimates the measured wind speeds. The slope of the regression between model and observations is 0.8 ($R^2$ = 0.68). This implies that the model slightly underestimates PMA emission fluxes, due to the wind speed dependence. This would be partly compensated by an overestimated wind speed dependence in the PMA-emission flux parameterisation by Long et al. (2011). There the authors assumed all air, which is entrained into the ocean, detrains as bubbles. As mentioned above, a part of the air dissolves in the ocean during the raise back to the surface leading to a lower amount of air detraining by bubbles than entrained by wave breaking.

### 4.1 Comparison of modelled sea salt aerosol with station data

The model results for sodium concentrations were compared with the measurements from the two EMEP-intensive campaigns in January 2007 and June 2006 (Figs. 6 and 8). The measurements (black symbols) are shown together with the model results neglecting a SST-dependence (blue lines) and using the S11-SST-correction (red lines). In all figures the EMEP-stations are sorted from north to south for January 2007 and June 2006.

To compare the model results for coarse mode particles, $PM_{10}$–$PM_{2.5}$ were calculated from $PM_{10}$ and $PM_{2.5}$ data (Fig. 6). It should be noted that the measurement uncertainties of $PM_{10}$–$PM_{2.5}$ thus contain the uncertainties of both measurements. $PM_{10}$–$PM_{2.5}$ measurement data show 2–3 times higher sodium concentrations at Auchencorth Moss, Cabauw and Melpitz in winter compared to summer. This can be attributed to the higher wintertime wind speed (Tsyro et al., 2011), which is the dominating parameter for PMA emissions. The salting of icy roads may also have an influence on the wintertime measurements, but is assumed to be of less importance (Tsyro et al., 2011). The measured sodium concentration at Virolahti is by a factor of 0.7 lower in January compared to June. This points to the importance of SST, which varies strongly in the Baltic Sea (near Virolahti) by up to a factor of 6 between January and June. At other stations it varies only by 1.8 (Irish Sea) to 3.2 (German Bay). Near Virolahti





ACPD
14, 377–434, 2014



the monthly averaged wind speed (model) increased by 1.8 from June to January. At Birkenes there is also a slight decrease by a factor of 0.9 in the sodium concentration, which is attributed to the different origin of the air masses in January and June. In January the main wind direction is west to northwest, resulting in a long transport time over land, which leads to a higher amount of particles to be deposited before they reach the station. In June, the main wind direction varies in such way that a higher amount of particles is advected from south to east, where transport over land is short. The highest monthly averaged sodium concentrations ($0.69\,\mu g\,m^{-3}$) are found at Cabauw in January. While the concentrations at Auchencorth Moss are clearly higher than at the inland station Melpitz with $0.63\,\mu g\,m^{-3}$ to $0.4\,\mu g\,m^{-3}$ in January, they are nearly equal in June with $0.26\,\mu g\,m^{-3}$ to $0.2\,\mu g\,m^{-3}$. The low sodium concentration ($0.15\,\mu g\,m^{-3}$ in January and $0.22\,\mu g\,m^{-3}$ in June) at Virolahti, which is comparable to or lower than at Melpitz, results from the low salinity of the Baltic Sea impacting PMA at Virolahti. In contrast, Melptiz is influenced by air masses from the Atlantic Ocean and North Sea. The model results with the uncorrected SS source function overestimate the concentration at nearly all stations and fit only at a few points well to the measurements. The SST-correction using S11 leads to a better agreement between model results and measurements with a tendency to underestimate the measured concentration at some points, especially at peak concentrations.

The $PM_{2.5}$ sodium concentrations in Fig. 7 show comparable features to $PM_{10}$–$PM_{2.5}$ with higher monthly averaged concentrations for Auchencorth Moss (3.0 times), Cabauw (1.8 times) and Melpitz (2.6 times) in winter than in summer. While the monthly average concentration at Virolahti in June is nearly equal to that in January, at Birkenes the concentration is by a factor of 3.2 lower in June compared to January, which is the highest factor for all 5 stations; and in contrast to $PM_{10}$–$PM_{2.5}$ where the wintertime concentration were slightly lower. This may be due to the lower deposition velocities of the smaller particles resulting in higher concentration in January, although the air mass travels a longer way over land. Once again the highest average concentration is found at Cabauw with $1\,\mu g\,m^{-3}$ in January and the lowest at Virolahti and Melpitz with





ACPD
14, 377–434, 2014



$0.11\,\mu g\,m^{-3}$ and $0.1\,\mu g\,m^{-3}$ in June, whereas Birkenes has also a low concentration in June with $0.12\,\mu g\,m^{-3}$. In January the concentration at Virolahti is the lowest with $0.11\,\mu g\,m^{-3}$. Again the SST-correction by S11 decreases the modelled sodium concentration, but less than for $PM_{10}$–$PM_{2.5}$. The overestimation using the uncorrected source function is decreased or disappeared at all stations, so the S11-SST-correction tends to underestimate the sodium concentration at some points.

$PM_1$ concentration data were only available at the stations Virolahti and Melpitz from January 2007 and June 2006 (Fig. 8). At both stations the measured concentrations are lower in June than in January with 0.77 and 0.87 in the monthly averaged values. In both months the sodium concentration is nearly 4.6 times higher at Melpitz than at Virolahti. Again this is due to the air mass origin (the low salinity in the Baltic Sea causing less SS in Virolahti) and the low deposition rate of the small particles, which causes less $PM_1$ removal compared to $PM_{10}$ removal. The S11-SST-correction function lowers the $PM_1$ concentration compared to the uncorrected version.

Figure 9 compares the model results for sodium with measurements by a Berner-impactor which operated at Sao Vincente. The measured sodium concentration increases from the second to the fifth impactor stage. The higher concentration in the first stage compared to the second were found in other measurements at this station as well (compare Müller et al., 2010) and may be due to higher uncertainties in the measurements at these low sodium concentrations. The model results with the S11-SST-correction are only a little lower than the uncorrected results, which is much less than the difference at the EMEP-stations due to the higher SST in the subtropical Atlantic ($\sim 20^{\circ}C$). At the second impactor stage both model versions slightly overestimate the measurements, while at the third to fifth stage both fit well, where S11 fits slightly better.





ACPD
14, 377–434, 2014



### 4.2 Contribution of organic matter to PMA

The contribution of primary OM to PMA is evaluated for the "African" domain in December 2007. This OM is emitted from the ocean surface mixed with SS. Figure 10 shows the monthly averaged emission fluxes of organic carbon (OC) obtained with the SST-correction function of S11. A conversion factor of 2 (Müller et al., 2010; Turpin et al., 2000), which stands for aged aerosol, was applied to obtain the OC mass from the modelled OM. The total amount of OC is found to be up to 3 times higher in the emitted submicron particles than in the supermicron particles. A maximum emission flux of $9\,\mathrm{ng\,m^{-2}\,s^{-1}}$ was found west of Great Britain. In this area high wind speeds often occur, especially in wintertime. The OC flux distribution shown in Fig. 10 indicates that the distribution of the OC emission is more strongly influenced by the wind speed, due to the correlation to the SS emission flux, than by the chlorophyll *a* concentration (compare Fig. 4). An inversely proportional wind speed dependence of the $R_{Vp}$ ratio, due to stronger ocean surface mixing and surface microlayer destruction at higher wind speeds (Gantt et al., 2011), would lower the influence of the wind speed on the total OC emission rate.

The locally increased emission fluxes west of Africa are due to the higher chlorophyll *a* concentration, which is a result of the increased primary production supported by high nutrient availability due to upwelling at the African west coast and the deposition of mineral dust from the Sahara. This region is important for the measurements at Sao Vincente since the majority of the detected air masses originate there. This leads to the daily averaged contribution of OM in the total PMA, shown in Fig. 11 for all 5 impactor stages at Sao Vincente. From the second to the fifth stage the measured $R_{Vp}$ decrease from 0.95 to 0.25, which is captured by the model. The lower ratio in stage 1 compared to stage 2 can be related to the higher sodium concentration in stage 1. Compared to the measurements the modelled $R_{Vp}$ shows much less variability at all sizes. This variability is due to the slightly different origins of the PMA with different chlorophyll *a* concentration. The inclusion of a wind speed dependence in computation





ACPD
14, 377–434, 2014



of the contribution of OM to total PMA and the use of daily resolved chlorophyll *a* concentration instead of the monthly averaged values may cause higher variability in the modelled $R_{Vp}$. The comparison of the model results with the measurements shows that the parameterisation of Long et al. (2011) in the current setup retrieves OM volume ratios, which underestimate the measurements at the four larger impactor stages. Likely this underestimation is a result of underestimating the total OM concentration, since the sodium concentration is in good agreement with the measurements (Fig. 9). This seems to be in contrast to the results of Gantt et al. (2012b), who found the parameterisation by Long et al. (2011) overpredicts the concentration of OM at Mace Head (53.33° N, 9.90° W) and Amsterdam Island (37.80° S, 77.57° E). However, those results were compared to stations in the mid-latitudes, while here the results are compared to a station in the lower latitudes (Table 2). Also, the model assumptions differ from each other, so that the results are not directly comparable. The differing results highlight the importance of the model set up to account for the correct description of the emission rates.

### 4.3 Emission fluxes

For the two simulations in January 2007 and June 2006 the monthly averaged emission fluxes of dry submicron and supermicron PMA mass are plotted in Fig. 12. There the results without temperature correction are shown. Due to the higher wind speeds in winter especially over the Atlantic the emission rates as well as the maximum emissions are higher in January than in June, resulting in higher airborne particle concentrations. This model result reproduces the majority of the measurements (compare Figs. 6 and 7). The location of the highest emission rates differs between January and June as well. While in June the areas with the local maximal emission rates are located north west of Ireland and west of Iceland, in January the maximum emission is spread over a larger area west of Ireland and Scotland with additional strong emissions from the North Sea. The low emission rates at the Baltic Sea are due its low salinity.





ACPD
14, 377–434, 2014



The SST correction factors applied to the emission fluxes are recalculated from the monthly averaged total emission fluxes for submicron and for supermicron particles (Figs. 13 and 14). The factors for all size classes differ more or less strongly from each other with the majority retrieving a factor lower than 1, thus decreasing the emission rates. The emission fluxes of supermicron particles are decreased by all parameterisations. The strongest decrease was found for S11, while the highest correction factors are found for the Zb13 starting north of Great Britain, because the emissions were unaffected above $T_W = 13^{\circ}C$ in that parameterisation. Apart from reducing emissions, none of the correction functions changes the regional characteristics of the emission fluxes, which remains dominated by the wind speed. J11 and S11 show the same characteristics in the submicron size fraction of PMA. The correction factor from J11 is identical for the submicron and supermicron particles, due to the missing size dependence. The submicron correction factor for S11 is higher than for supermicron particles but still below 1. This is despite the fact that the S11-SST-correction function showed an increase in the emission rates of small particles (see Fig. 1). However, since it decreases emissions for particles larger than 0.2 µm which dominate the mass of submicron particles this leads to the decrease of the total emission fluxes with temperature. Finally the Zb13-SST-correction function increases the submicron emissions for lower SST. This is because of the high factor for particles around 0.1 micron, which then dominate the size distribution. This high factor leads to changed regional characteristics of the highest PMA emission rates, which are now located at the low temperature water around Greenland. Furthermore the high correction factors at the northern Baltic Sea should be noted, which lead to strong increases in the emission rates resulting in high concentrations at Virolahti when using this function.

### 4.4 Sensivity to correction of the SST

The Figs. 15–18 show boxplots with the 5, 25, 50, 75 and 95-percentile for the measurements compered to the median of the model results, where S11 is given in red symbols, J11 in black symbols, Zb13 in green symbols and the results without SST





ACPD
14, 377–434, 2014



correction in blue symbols. The daily average values are used for all included data and only these model values were taken into account where measurements exist.

#### 4.4.1 $PM_{10}$–$PM_{2.5}$

For $PM_{10}$–$PM_{2.5}$ concentrations the measurements and model results at the five EMEP-stations are plotted in Fig. 15. As explained above, the model simulates the highest sodium concentrations when using no correction for SST. All SST-correction functions lower the modelled concentrations, with Zb13 resulting in the highest and S11 the lowest values. The uncorrected values are higher than the measured ones at all stations and higher or even near the 95-percentile at the majority of the stations especially in January. For Virolahti, Birkenes and Melpitz in June the uncorrected concentrations are closer to the measured median and within the 75-percentile. The higher overprediction in January points towards the need of the SST correction. All three tested correction functions improved the model results compared to the measurements. While Zb13 and J11 lower the concentrations only a little so that there are still stations with overprediction of sodium concentrations, the S11-SST-correction function lead to underestimations of the modelled concentrations except at Auchencorth Moss and Birkenes in January, but overall the S11-SST-correction result in the best agreement of model results and observations.

#### 4.4.2 $PM_{2.5}$

Boxplots of $PM_{2.5}$ are shown for the same stations as for $PM_{10}$–$PM_{2.5}$ (Fig. 16). In that size range no clear optimum correction function is found. The Zb13-SST-correction function increases the concentrations, because the correction factor is higher than 1 for particles smaller than 1.8 µm. This leads to worse results where the uncorrected version overpredicts the measured concentration, but improves the results at Cabauw, Auchencorth Moss in January and Melpitz in June. Since the results of the uncorrected model are close to the measurements, the S11-SST-correction function leads to strong





ACPD
14, 377–434, 2014



underpredictions of the measurements. Overall the J11-SST-correction function tends to result in best agreement with measurements for that case study.

#### 4.4.3 $PM_1$

It was mentioned above that the SST-correction with Zb13 retrieves high correction factors for $PM_1$ at the northern Baltic Sea. This leads to high emission rates resulting in high modelled concentrations of marine aerosol at the station Virolahti. In Fig. 17 it can be seen that these high values lead to a strong overprediction of the sodium mass compared to the measurements, especially in January. The lower concentrations by the neglection of the SST-dependence or the use of S11 and J11 are closer to the measurements for that station. However these three model setups underpredicted the concentration at Melpitz, where the increase of the concentration by Zb13 fits best to the measurements.

#### 4.4.4 Berner-impactor at Sao Vicente

Figure 18 compares the model results with measurements of a Berner-impactor which operated at the CVAO at Sao Vincente. Due to the relatively high SST at these latitudes only a slight influence by the correction functions can be distinguished. S11 shows the strongest decrease in the concentrations, caused by the origin of the air mass, which is mainly from regions with a SST around 20 °C. J11 does not change the concentrations compared to the uncorrected version significantly and Zb13 has no influence due to the SST being above 13 °C.

For the second, fourth and fifth stage best agreement is for S11, but again with the tendency to underestimate the concentration. For the third stage it cannot be decided which parameterisation results in the best values in comparison with the measurements.





ACPD
14, 377–434, 2014



## 5 Discussion

The EMEP-intensive campaign measurements were also used by Tsyro et al. (2011) for the evaluation of the EMEP chemical transport model. The authors found the model to underpredict the $PM_{2.5}$ and $PM_{10}$ sodium concentration in June 2006 while the model underprediction is less or changes to overprediction of the measurements in January 2007. They attributed the discrepancies to inaccuracies in the wind prediction or the coarse model grid resolution (50 km × 50 km). The same results are found for sodium concentrations for COSMO-MUSCAT when PMA emissions are not SST corrected (Figs. 6 and 7). In contrast to the EMEP-model the sodium concentration is overestimated with the uncorrected SS source function in COSMO-MUSCAT. SST correction of the PMA emission decreases the modelled sodium concentration at the EMEP stations, so that the measurements are matched better than without correction. This is particularly evident for the $PM_{10}$–$PM_{2.5}$ size range and for the winter month. The strongest emission decrease was obtained by S11 resulting in underestimation of the sodium concentration at the measurement sites, while the J11-SST-correction has a smaller effect. For the coarse particles the use of the SST-correction function by S11 gives reasonable results.

The effect of the SST correction is not as clear for $PM_{2.5}$ concentrations. For this size range the S11-SST-correction function leads to worse results compared to the other functions in the comparison with the observations. In the current work the parameterisation of Long et al. (2011) was used to describe the PMA emission flux. The use of a different PMA emission functions (e.g., Sofiev et al., 2011) (Fig. 2) with higher emission rates will result in higher non-SST-corrected $PM_{2.5}$ sodium concentrations than with the parameterization by Long et al. (2011). In combination with the S11-SST-correction those modelled concentrations would result in better agreement with the observations at the EMEP measurement sites, but would lead to overestimations of the concentrations at Sao Vincente.





ACPD
14, 377–434, 2014



At Melpitz, the measured sodium concentrations in the $PM_1$ size range decrease in January compared to June. This is in contrast to coarse particles, where they increase. This behaviour is similar for Virolahti, but less clear. Such an effect could be due to the decrease of the concentration of larger particles within the size spectrum being partly compensated by the increase of smaller particles with lower SST. However, the evaluation at only two stations and two months is insufficient to obtain statistically meaningful results. In general, the uncorrected version tends to underestimate the $PM_1$ concentration so that the results with Zb13 are in best agreement with the measurements at the EMEP station. However, the very high correction factor for low temperatures leads to overestimations of the concentration at near coastal stations in winter as at Virolahti. Based on the small amount of available measurement data, a final conclusion for the SST-correction function regarding $PM_1$ is not possible.

The measured sodium concentration at Virolahti is low compared to Cabauw or Auchencorth Moss, although all stations are of marine background. The reason for this is the air mass origin – Virolahti is influenced by air masses from the Baltic Sea, which has a salinity of 7‰ and lower. In contrast, the air mass arriving at Cabauw and Auchencorth Moss originates from the North Sea and the north-east Atlantic, where the salinity is around 35‰. The model captures the influence of salinity on SSA emission well.

The new SST-correction function that was based on measurements by Zábori et al. (2012) did not lead to better results compared to the other parameterizations. With that parameterization the concentrations of fine particles were overpredicted especially near cold waters, and the decrease of the coarse particle concentration was too low to reproduce the measured concentration. The size dependence of the correction factor cannot be validated by the available measurements.

The modelled monthly averaged emission fluxes of submicron primary OC for the "African" model domain in December 2007 were found to be between 1–2 $ng\,m^{-2}\,s^{-1}$ west of Africa and the Mediterranean Sea and increase west of Europe towards





ACPD
14, 377–434, 2014



$9\,ng\,m^{-2}\,s^{-1}$ west of Great Britain. This is comparable to the multi-year average values determined by Long et al. (2011) and Spracklen et al. (2008).

## 6 Conclusions

In this work we tested the importance of considering the influence of SST on PMA emissions, together with impacts of surface winds and salinity. In particular for coarse mode particles neglecting the SST-dependence lead to overestimations of the PMA-concentrations by the model compared to measurements at land and island stations. While we find that using the correction functions by S11 and J11 improve the model performance for coarse mode particles, not enough data were available for $PM_1$ to test the role of SST in this size fraction. More measurements in this size range are required to study particle fluxes in the small sizes that are also important to study the role of PMA in cloud modification.

A size shift of the dry SSA size distribution towards smaller sizes with lower salinities could be indicated.

For the description of the contribution of OM to PMA a replacement of SS by this OM has been assumed in the combination with the Long et al. (2011) function for the description of the their relation to each other. While the monthly averaged emission rates for submicron OM in December 2007 were found to be comparable to multi-year averaged values from literature, the measured ratio of OM to total PMA were underestimated at Sao Vincente. Since the used parameterization was developed from laboratory measurements it accounts only for primary OM. However secondary OM may also be part of the detected aerosols, leading to underestimations by the model results. Furthermore OM from the African continent can be detected within the measurements, which has also not been taken into account in the model. Both factors need to be discussed in future works.

*Acknowledgements.* This work was supported by the German Science Foundation (DFG) (Grant No. TG 376/6-1) and by the BMBF (Bundesministerium für Bildung und Forschung)





ACPD
14, 377–434, 2014



as part of the SOPRAN project (FZK 03F0611J) which is a German national contribution to the international SOLAS project.

Special thanks to the NASA for providing the chlorophyll *a* database on the OceanColor webpage and NOAA for the salinity database as part of the World Ocean Atlas 2001.

The authors thank Jan Erik Hanssen, Gerald Spindler, Timo Salmi Chiara DiMarco and the colleagues from RIVM (National Institute for Public Health and the Environment Centre for Environmental Quality) (the Netherlands) for their work on the measurement data as well as the colleagues from the Norwegian Institute for Air Research for publishing the collection of all measurement data on the EBAS webpage.

## References

Andreas, E. L.: A new sea spray generation function for wind speeds up to 32 m s$^{-1}$, J. Phys. Oceanogr., 28, 2175–2184, doi:10.1175/1520-0485(1998)028<2175:ANSSGF>2.0.CO;2, 1998. 380, 387

Barker, D. R. and Zeitlin, H.: Metal-ion concentrations in seasurface microlayer and size separated atmospheric aerosol samples in Hawaii, J. Geophys. Res., 77, 5076–5086, doi:10.1029/JC077i027p05076, 1972. 382

Blanchard, D. C.: The electification of the atmosphere by particles from bubbles in the sea, in: Progress in Oceanography, vol. 1, chap. 2, Elsevier, New York, 1963. 380, 384

Blanchard, D. C.: Sea-to-air transport of surface active material, Science, 146, 396–397, doi:10.1126/science.146.3642.396, 1964. 382

Blanchard, D. C.: The Production, Distribution, and Bacterial Enrichment of the Sea-Salt Aerosol, D. Reidel, Dordrecht, 407–454, 1983. 381

Bowyer, P. A., Woolf, D. K., and Monahan, E. C.: Temperature dependence of the charge and aerosol production associated with a breaking wave in a whitecap simulation tank, J. Geophys. Res.-Oceans, 95, 5313–5319, doi:10.1029/JC095iC04p05313, 1990. 384, 385, 389

Carlson, D. J.: Dissolved organic materials in surface microlayers: temporal and spatial variability and relation to sea state, Limnol. Oceanogr., 28, 415–431, 1983. 382

Chen, S. F., Chan, R. C., Read, S. M., and Beomley, L. A., Viscosity of sea water solutions, Desalination, 13, 37–51, 1973. 383





ACPD
14, 377–434, 2014



Clarke, A. D., Owens, S. R., and Zhou, J.: An ultrafine sea-salt flux from breaking waves: implications for cloud condensation nuclei in the remote marine atmosphere, J. Geophys. Res., 111, D06202, doi:10.1029/2005JD006565, 2006. 381, 387, 389

de Leeuw, G., Andreas, E. L., Anguelova, M. D., Fairall, C. W., Lewis, E. R., O'Dowd, C., Schulz, M., and Schwartz, S. E.: Production flux of sea spray aerosol, Rev. Geophys., 49, RG2001, doi:10.1029/2010RG000349, 2011. 387

Duce, R. A. and Hoffmann, E. J.: Chemical fractionation at the air/sea interface, Annu. Rev. Earth Pl. Sc., 4, 187–228, 1976. 382

Facchini, M. C., Rinaldi, M., Decesari, S., Carbone, C., Finessi, E., Mircea, M., Fuzzi, S., Ceburnis, D., Flanagan, R., Nilsson, E. D., de Leeuw, G., Martino, M.,Woeltjen, J., and O'Dowd, C. D.: Primary submicron marine aerosol dominated by insoluble organic colloids and aggregates, Geophys. Res. Lett., 35, L17814, doi:10.1029/2008GL034210, 2008. 389

Fan, T. and Toon, O. B.: Modeling sea-salt aerosol in a coupled climate and sectional microphysical model: mass, optical depth and number concentration, Atmos. Chem. Phys., 11, 4587–4610, doi:10.5194/acp-11-4587-2011, 2011. 379, 389

Fuentes, E., Coe, H., Green, D., de Leeuw, G., and McFiggans, G.: On the impacts of phytoplankton-derived organic matter on the properties of the primary marine aerosol – Part 1: Source fluxes, Atmos. Chem. Phys., 10, 9295–9317, doi:10.5194/acp-10-9295-2010, 2010. 379, 382

Gantt, B. and Meskhidze, N.: The physical and chemical characteristics of marine primary organic aerosol: a review, Atmos. Chem. Phys., 13, 3979–3996, doi:10.5194/acp-13-3979-2013, 2013. 382, 383, 392

Gantt, B., Meskhidze, N., Facchini, M. C., Rinaldi, M., Ceburnis, D., and O'Dowd, C. D.: Wind speed dependent size-resolved parameterization for the organic mass fraction of sea spray aerosol, Atmos. Chem. Phys., 11, 8777–8790, doi:10.5194/acp-11-8777-2011, 2011. 382, 398

Gantt, B., Xu, J., Meskhidze, N., Zhang, Y., Nenes, A., Ghan, S. J., Liu, X., Easter, R., and Zaveri, R.: Global distribution and climate forcing of marine organic aerosol – Part 2: Effects on cloud properties and radiative forcing, Atmos. Chem. Phys., 12, 6555–6563, doi:10.5194/acp-12-6555-2012, 2012a. 379, 382

Gantt, B., Johnson, M. S., Meskhidze, N., Sciare, J., Ovadnevaite, J., Ceburnis, D., and O'Dowd, C. D.: Model evaluation of marine primary organic aerosol emission schemes, Atmos. Chem. Phys., 12, 8553–8566, doi:10.5194/acp-12-8553-2012, 2012b. 382, 390, 399





ACPD
14, 377–434, 2014



Gong, S. L.: A parameterization of sea-salt aerosol source function for sub- and super-micron particles, Global Biogeochem. Cy., 17, 1097, doi:10.1029/2003GB002079, 2003. 381, 387, 388

Grini, A., Myhre, G., Sundet, J. K., and Isaksen, I. S. A.: Modeling the annual cycle of sea salt in the Global 3-D Model Oslo CTM2, concentrations, fluxes and radiative impact, J. Climate, 15, 1717–1730, doi:10.1175/1520-0442(2002)015<1717:MTACOS>2.0.CO;2, 2002. 379

Hardy, J. T.: The sea surface microlayer: biology, chemistry and antropogenic emnrichment, Prog. Oceanogr., 11, 307–328, 1982. 382

Haywood, J. M., Ramaswamy, V., and Soden, B. J.: Tropospheric aerosol climate forcing in clear-sky satellite observations over the oceans, Science, 283, 1299–1303, doi:10.1126/science.283.5406.1299, 1999. 379

Heinold, B., Tegen, I., Bauer, S., and Wendisch, M.: Regional modelling of Saharan dust and biomass-burning smoke, Tellus B, 63, 800–813, doi:10.1111/j.1600-0889.2011.00574.x, 2011. 390, 393

Hoffman, E. J. and Duce, R.: Organic carbon in marine atmospheric particulate matter: concentration and particle size distribution, Geophys. Res. Lett., 4, 449–452, doi:10.1029/GL004i010p00449, 1977. 382

Hoppel, W. A., Caffrey, P. F., and Frick, G. M., Particle deposition on water: surface source versus upwind source, J. Geophys. Res., 110, D10206, doi:10.1029/2004JD005148, 2005. 389

Hultin, K. A. H., Krejci, R., Pinhassi, J., Gomez-Consarnau, L., Mårtensson, E. M., Hagström, Å., and Nilsson, E. D.: Aerosol and bacterial emissions from Baltic seawater, Atmos. Res., 99, 1–14, doi:10.1016/j.atmosres.2010.08.018, 2011. 384, 385

Jaeglé, L., Quinn, P. K., Bates, T. S., Alexander, B., and Lin, J.-T.: Global distribution of sea salt aerosols: new constraints from in situ and remote sensing observations, Atmos. Chem. Phys., 11, 3137–3157, doi:10.5194/acp-11-3137-2011, 2011. 378, 379, 380, 385

Keene, W. C., Maring, H., Kieber, D. J., Maben, J. R., Pszenny, A. A. P., Dahl, E. E., Izaguirre, M. A., Davis, A. J., Long, M. S., Zhou, X., Smoydzin, L., von Glasow, R., and Sander, R.: Chemical and physical characteristics of nascent aerosols produced by bursting bubbles at a model air–sea interface, J. Geophys. Res., 112, D21202, doi:10.1029/2007JD008464, 2007. 381, 389, 392





ACPD
14, 377–434, 2014



Lewis, E. R. and Schwartz, S. E.: Sea Salt Aerosol Production: Mechanisms, Methods, Measurements and Models: a Critical Review, American Geophysical Union, Washington D.C., 2004. 379, 380, 381, 382, 384

Lewis, E. R. and Schwartz, S. E.: Comment on "size distribution of sea-salt emissions as a function of relative humidity?", Atmos. Environ., 40, 588–590, doi:10.1016/j.atmosenv.2005.08.043, 2006. 392

Long, M. S., Keene, W. C., Kieber, D. J., Erickson, D. J., and Maring, H.: A sea-state based source function for size- and composition-resolved marine aerosol production, Atmos. Chem. Phys., 11, 1203–1216, doi:10.5194/acp-11-1203-2011, 2011. 382, 387, 388, 389, 390, 391, 395, 399, 403, 405

Lundgren, K., Vogel, B., Vogel, H., and Kottmeier, C.: Direct radiative effects of sea salt for the Mediterranean region under conditions of low to moderate wind speeds, J. Geophys. Res. Atmos., 118, 1906–1923, doi:10.1029/2012JD018629, 2013. 379, 387

Ma, X., von Salzen, K., and Li, J.: Modelling sea salt aerosol and its direct and indirect effects on climate, Atmos. Chem. Phys., 8, 1311–1327, doi:10.5194/acp-8-1311-2008, 2008. 379

Mårtensson, E. M., Nilsson, E. D., de Leeuw, G., Cohen, L. H., and Hansson, H.-C.: Laboratory simulations and parameterization of the primary marineaerosol production, J. Geophys. Res., 108, 4297, doi:10.1029/2002JD002263, 2003. 379, 381, 384, 385, 386, 387, 389

Maria, S. F., Russell, L. M., Gilles, M. K., and Myneni, S. C. B.: Organic aerosol growth mechanisms and their climate-forcing implications, Science, 306, 1921–1924, doi:10.1126/Science.1103491, 2004. 392

Meskhidze, N., Xu, J., Gantt, B., Zhang, Y., Nenes, A., Ghan, S. J., Liu, X., Easter, R., and Zaveri, R.: Global distribution and climate forcing of marine organic aerosol: 1. Model improvements and evaluation, Atmos. Chem. Phys., 11, 11689–11705, doi:10.5194/acp-11-11689-2011, 2011. 379, 382

Modini, R. L., Russel, L. M., Deane, G. B., and Stokes, M. D.: Effect of soluble surfactant on bubble-produced aerosol particles, J. Geophy. Res.-Atmos., 118, 1288–1400, doi:10.1002/jgrd.50186, 2013. 383

Monahan, E. C. and O'Muircheartaigh, I.: Optimal power-law description of oceanic whitecap coverage dependence on wind speed, J. Phys. Oceanogr., 10, 2094–2099, 1980. 381

Monahan, E. C., Fairall, C. W., Davidson, K. L., and Boyle, P. J.: Observed inter-relations between 10 m winds, ocean whitecaps and marine aerosols, Q. J. Roy. Meteor. Soc., 109, 379–392, 1983. 380





ACPD
14, 377–434, 2014



Monahan, E. C., Spiel, D. E., and Davidson, K. L.: A model of marine aerosol generation and wave disruption, in: Oceanic Whitecaps and Their Role in Air–Sea Exchange Processes, edited by: Monahan, E. C. and MacNoicaill, G., Springer, New York, 167–174, 1986. 381, 387, 389, 392

Müller, K., Lehmann, S., van Pinxteren, D., Gnauk, T., Niedermeier, N., Wiedensohler, A., and Herrmann, H.: Particle characterization at the Cape Verde atmospheric observatory during the 2007 RHaMBLe intensive, Atmos. Chem. Phys., 10, 2709–2721, doi:10.5194/acp-10-2709-2010, 2010. 393, 397, 398

Müller, T., Schladitz, A., Kandler, K., and Wiedensohler, A.: Spectral particle absorption coefficients, single scattering albedos and imaginary parts of refractive indices from ground based in situ measurements at Cape Verde Island during SAMUM-2, Tellus B, 63, 573–588, doi:10.1111/j.1600-0889.2011.00572.x, 2011. 393

Murphy, D. M., Anderson, J. R., Quinn, P. K., McInnes, L. M., Brechtel, F. J., Kreidenweis, S. M., Middlebrook, A. M., Posfai, M., Thomson, D. S., and Buseck, P. R.: Influence of sea-salt on aerosol radiative properties in the Southern Ocean marine boundary layer, Nature, 392, 6265, doi:10.1038/32138, 1998. 379

Nilsson, E. D., Rannik, Ü., Swietlicki, E., Leck, C., Aalto, P. P., Zhou, J., and Norman, M.: Turbulent aerosol fluxes over the Arctic Ocean: 2. Winddriven sources from the sea, J. Geophys. Res., 106, 32111–32124, doi:10.1029/2000JD900747, 2001. 381

Oceancolor: available at: http://oceancolor.gsfc.nasa.gov/, last access: 13 June 2012.

O'Dowd, C. D. and de Leeuw, G.: Marine aerosol production: a review of the current knowledge, Philos. T. Roy. Soc., 365, 1753–1774, doi:10.1098/rsta.2007.2043, 2007. 378

O'Dowd, C. D. and Smith, M. H.: Physicochemical properties of aerosols over the northeast Atlantic: evidence for wind-speed-related submicron sea-salt aerosol production, J. Geophys. Res., 98, 1137–1149, doi:10.1029/92JD02302, 1993. 379, 381

O'Dowd, C. D., Facchini, M. C., Cavalli, F., Ceburnis, D., Mircea, M., Decesari, S., Fuzzi, S., Yoon, Y. J., and Putaud, J.-P.: Biogenically driven organic contribution to marine aerosol, Nature, 431, 676–680, doi:10.1038/nature02959, 2004. 379, 382

Oppo, C., Bellandi, S., Degli Innocenti, N., Stortini, A. M., Loglio, G., Schiavuta, E., and Cini, R.: Surfactant components of marine organic matter as agents for biogeochemical fractionation and pollutant transport via marine aerosols, Mar. Chem., 63, 235–253, doi:10.1016/S0304-4203(98)00065-6, 1999. 382





ACPD
14, 377–434, 2014



Pierce, J. R. and Adams, P. J.: Global evaluation of CCN formation by direct emission of sea salt and growth of ultrafine sea salt, J. Geophys. Res., 111, D06203, doi:10.1029/2005JD006186, 2006. 379

Polarstern on www.awi.de: available at: http://www.awi.de/en/infrastructure/ships/polarstern/meteorological_observatory/continuous_measurements/sensor_information/, last access: 13 August 2013.

Pounder, C. D.: Sodium cloride and water temperature effects on bubbles, in: Oceanic Whitecaps and Their Role in Air–Sea Exchange Processes, edited by: Monahan, E. C. and Mac Nicaill, G., D. Reidel, Norwell, Mass., 278–279, 1986. 384

Pruppacher, H. R. and Klett, J. D.: Microphysics of Clouds and Precipitation, Kluwer Academic Publishers, Dordrecht, 1997. 378

Quinn, P. K., Coffman, D. J., Kapustin, V. N., Bates, T. S., and Covert, D. S.: Aerosol optical properties in the marine boundary layer during the first Aerosol Characterization Experiment (ACE 1) and the underlying chemical and physical aerosol properties, J. Geophys. Res., 103, 16547–16563, doi:10.1029/97JD02345, 1998. 379

Renner, E. and Wolke, R.: Modelling the formation and atmospheric transport of secondary inorganic aerosols with special attention to regions with high ammonia emissions, Atmos. Environ., 44, 1904–1912, doi:10.1016/j.atmosenv.2010.02.018, 2010. 390

Rinaldi, M., Facchini, M. C., Decesari, S., Carbone, C., Finessi, E., Mircea, M., Fuzzi, S., Ceburnis, D., Ehn, M., Kulmala, M., de Leeuw, G., and O'Dowd, C. D.: On the representativeness of coastal aerosol studies to open ocean studies: Mace Head – a case study, Atmos. Chem. Phys., 9, 9635–9646, doi:10.5194/acp-9-9635-2009, 2009. 382

Roelofs, G. J.: A GCM study of organic matter in marine aerosol and its potential contribution to cloud drop activation, Atmos. Chem. Phys., 8, 709–719, doi:10.5194/acp-8-709-2008, 2008. 379, 382

Russell, L. M., Hawkins, L. N., Frossard, A. A., Quinn, P. K., and Bates, T. S.: Carbohydrate-like composition submicron atmospheric particles and their production from ocean bubble bursting, P. Natl. Acad. Sci. USA, 107, 6652–6657, doi:10.1073/pnas.0908905107, 2010. 382

Schättler, U., Doms, G., and Schraff, C.: A Description of the Nonhydrostatic Regional COSMO-Model, Deutscher Wetterdienst, Offenbach, available at: http://www.cosmo-model.org, 2008. 390





ACPD
14, 377–434, 2014



Schulz, M., de Leeuw, G., and Balkanski, Y.: Sea-salt aerosol source functions and emissions, in: Emissions of Atmospheric Trace Compounds, edited by: Granier, C., Artaxo, P., and Reeves, C., Kluwer, Dordecht, the Netherlands, 333–359, 2004. 387

Sciare, J., Favez, O., Sarda-Estève, R., Oikonomou, K., Cachier, H., and Kazan, V.: Long-term observations of carbonaceous aerosols in the Austral Ocean atmosphere: evidence of a biogenic marine organic source, J. Geophys. Res., 114, D15302, doi:10.1029/2009JD011998, 2009. 382

Seinfeld, J. H. and Pandis, S. N.: Atmospheric Chemistry and Physics – from Air Pollution to Climate Change, 2nd Edn., John Wiley and Sons, New York, 2006. 391, 393

Sellegri, K., O'Dowd, C. D., Yoon, Y. J., Jennings, S. G., and de Leeuw, G.: Surfactants and submicron sea spray generation, J. Geophys. Res., 111, D22215, doi:10.1029/2005JD006658, 2006. 382, 383, 384, 387, 389

Smith, M. H. and Harrison, N. M.: The sea spray generation function, J. Aerosol Sci., 29, Supplement 1, S189–S190, doi:10.1016/S0021-8502(98)00280-8, 1998. 381, 389

Smith, M. H., Park, P. M., and Consterdine, I. E.: Marine aerosol concentrations and estimated fluxes over the sea, Q. J. Roy. Meteor. Soc., 119, 809–824, doi:10.1002/qj.49711951211, 1993. 381, 387, 389

Smoydzin, L. and von Glasow, R.: Do organic surface films on sea salt aerosols influence atmospheric chemistry? – a model study, Atmos. Chem. Phys., 7, 5555–5567, doi:10.5194/acp-7-5555-2007, 2007. 379

Spiel, D. E.: On the birth of film drops from bubbles bursting on seawater surfaces, J. Geophys. Res., 95, 18281–18288, 1998. 380

Spracklen, D. V., Arnold, S. R., Carslaw, K. S., Sciare, J., and Pio, C.: Globally significant oceanic source of organic carbon aerosol, Geophys. Res. Lett., 35, L12811, doi:10.1029/2008GL033359, 2008. 405

Sofiev, M., Soares, J., Prank, M., de Leeuw, G., and Kukkonen, J.: A regional-to-global model of emission and transport of sea salt particles in the atmosphere, J. Geophys. Res., 116, D21302, doi:10.1029/2010JD014713, 2011. 378, 379, 380, 385, 386, 387, 389, 403, 415

Textor, C., Schulz, M., Guibert, S., Kinne, S., Balkanski, Y., Bauer, S., Berntsen, T., Berglen, T., Boucher, O., Chin, M., Dentener, F., Diehl, T., Easter, R., Feichter, H., Fillmore, D., Ghan, S., Ginoux, P., Gong, S., Grini, A., Hendricks, J., Horowitz, L., Huang, P., Isaksen, I., Iversen, I., Kloster, S., Koch, D., Kirkevåg, A., Kristjansson, J. E., Krol, M., Lauer, A., Lamarque, J. F., Liu, X., Montanaro, V., Myhre, G., Penner, J., Pitari, G., Reddy, S., Seland, Ø., Stier, P.,





ACPD
14, 377–434, 2014



Takemura, T., and Tie, X.: Analysis and quantification of the diversities of aerosol life cycles within AeroCom, Atmos. Chem. Phys., 6, 1777–1813, doi:10.5194/acp-6-1777-2006, 2006. 379

Thrope, S. A., Bowyer, P., and Woolf, D. K.: Some factors affecting the size distributions of oceanic bubbles, J. Phys. Oceanogr., 22, 382–289, doi:10.1175/1520-0485(1992)022<0382:SFATSD>2.0.CO;2, 1992. 384

Tsyro, S. and Erdman, L.: Parameterization of Aerosol Deposition Proceses in EMEP MSC-E and MSC-W Transport Models, EMEP/MSC-E & MCS-WNote 7/00, Norwegian Meteorological Institute, Oslo, 2000. 391

Tsyro, S., Aas, W., Soares, J., Sofiev, M., Berge, H., and Spindler, G.: Modelling of sea salt concentrations over Europe: key uncertainties and comparison with observations, Atmos. Chem. Phys., 11, 10367–10388, doi:10.5194/acp-11-10367-2011, 2011. 379, 392, 393, 395, 403

Turpin, B. J., Saxena, P., and Andrews, E.: Measuring and simulating particulate organics in the atmosphere: problems and prospects, Atmos. Environ., 34, 2983–3013, doi:10.1016/S1352-2310(99)00501-4, 2000. 398

von Glasow, R., Sander, R., Bott, A., and Crutzen, P. J.: Modeling halogen chemistry in the marine boundary layer, 1. Cloudfree MBL, J. Geophys. Res., 107, 4341, doi:10.1029/2001JD000942, 2002. 379

Westervelt, D. M., Moore, R. H., Nenes, A., and Adams, P. J.: Effect of primary organic sea spray emissions on cloud condensation nuclei concentrations, Atmos. Chem. Phys., 12, 89–101, doi:10.5194/acp-12-89-2012, 2012. 379, 382

Wolke, R., Schröder, W., Schrödner, R., and Renner, E.: Influence of grid resolution and meteorological forcing on simulated European air quality: a sensitivity study with the modeling system COSMO-MUSCAT, Atmos. Environ., 53, 110–130, doi:10.1016/j.atmosenv.2012.02.085, 2012. 390, 391

World Ocean Atlas 2001: available at: www.nodc.noaa.gov/OC5/WOA01/qd_ts01.html, last access: 4 May 2011.

Wu, J.: Oceanic whitecaps and sea state, J. Phys. Oceanogr., 9, 1064–1068, doi:10.1175/1520-0485(1979)009<1064:OWASS>2.0.CO;2, 1979. 382

Yttri, K.-E., Aas, W., Tørseth, K., Stebel, K., Nyíri, Á., Tsyro, S., Merckova, K., Wankmüller R., Winiwarter, W., Bauer, H., Caseiro, A., Puxbaum, H., Holzer-Popp, T., and Schroedter-





ACPD
14, 377–434, 2014



Homscheidt, M.: Transboundary particulate matter in Europe, Status report 2008, Joint CCC & MSC-W & CEIP report 2008, Oslo, 2008. 392

Zábori, J., Matisäns, M., Krejci, R., Nilsson, E. D., and Ström, J.: Artificial primary marine aerosol production: a laboratory study with varying water temperature, salinity, and succinic acid concentration, Atmos. Chem. Phys., 12, 10709–10724, doi:10.5194/acp-12-10709-2012, 2012. 380, 384, 385, 386, 387, 389, 404





ACPD
14, 377–434, 2014



**Table 1.** Parameters for Eq. (5) by Sofiev et al. (2011).

| Temperature/°C | *a* | *b* |
|---|---|---|
| −2 | 0.092 | −0.96 |
| 5 | 0.15 | −0.88 |
| 15 | 0.48 | −0.36 |
| 25 | 1 | 0 |





ACPD
14, 377–434, 2014



**Table 2.** Geographical position of the stations used for model evaluation.

| Station | Country | Latitude | Longitude |
|---|---|---|---|
| Virolahti II | Finland | 60.527° N | 27.686° E |
| Birkenes | Norway | 58.383° N | 8.25° E |
| Auchencorth Moss | Great Britain | 55.793° N | 3.245° W |
| Cabauw | Nertherlands | 51.97° N | 4.93° E |
| Melpitz | Germany | 51.53° N | 12.93° E |
| Sao Vincente | Cape Vede | 16.864° N | 24.417° W |





ACPD
14, 377–434, 2014



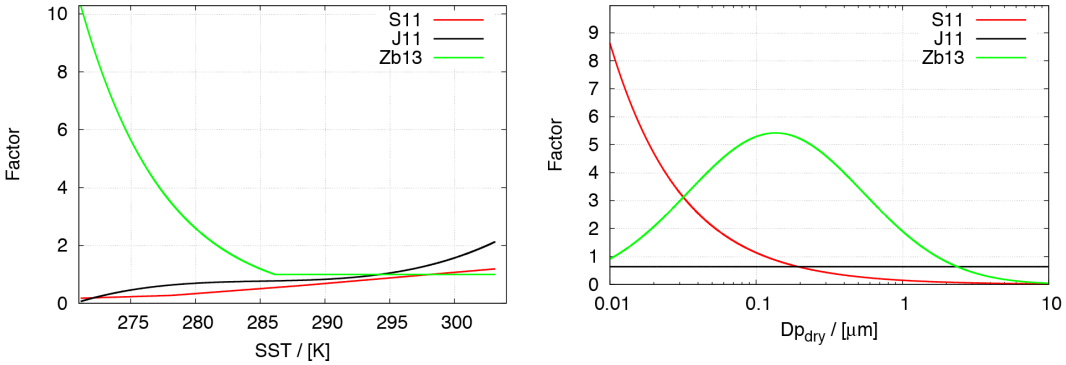


**Fig. 1.** Temperature dependence and size distribution of three functions for the SST correction factor for particles with a dry particle diameter $D_p$ = 500 nm (left) and for a SST of 5 °C (right).





ACPD
14, 377–434, 2014



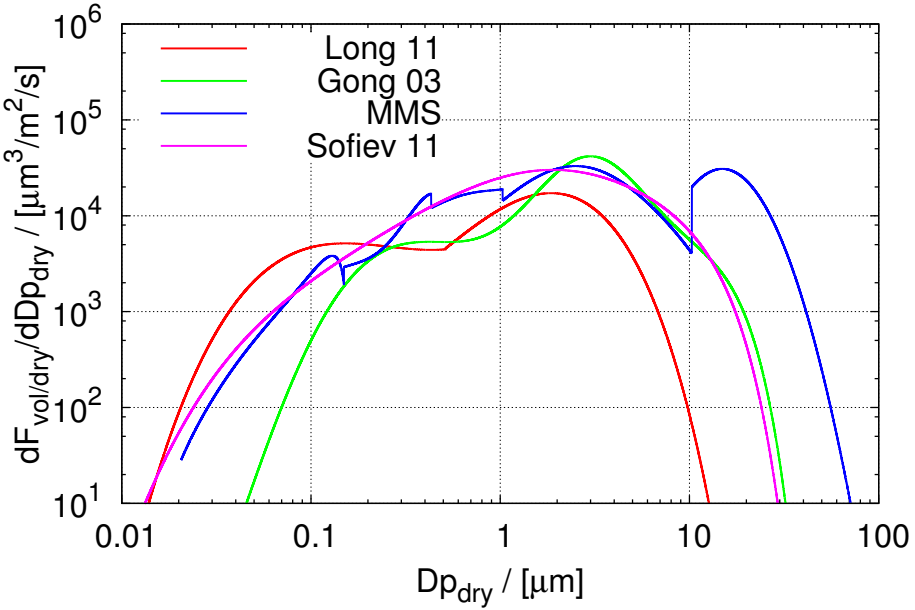


**Fig. 2.** Effective PMA volume emission flux at 10 m height for 4 sea salt source functions for dry SSA at a 10 m-windspeed of $U_{10} = 10\,\mathrm{m\,s^{-1}}$, a salinity of $s = 35‰$ and a SST of $T_W = 25^\circ\mathrm{C}$.





ACPD
14, 377–434, 2014



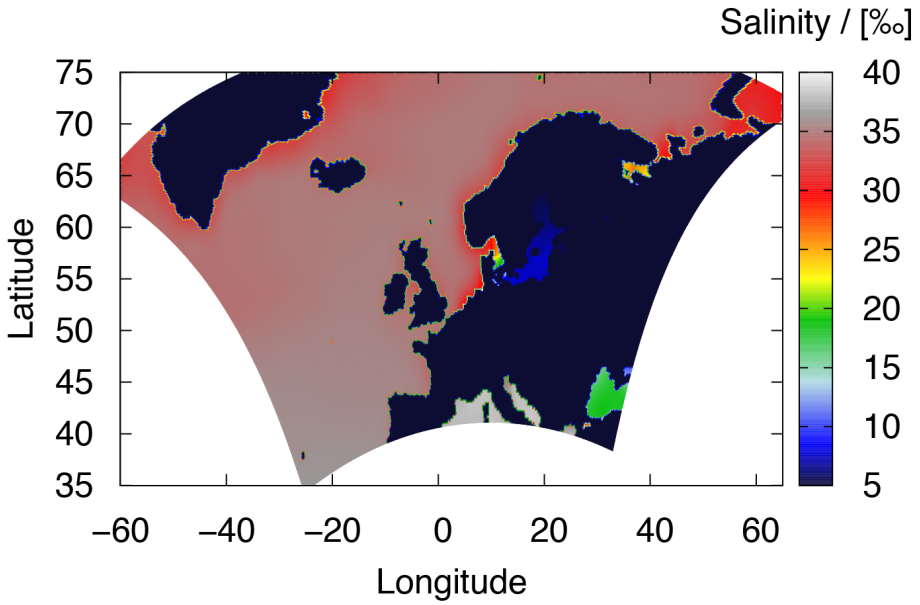


**Fig. 3.** Yearly averaged surface salinity data from World Ocean Atlas 2001.





ACPD
14, 377–434, 2014



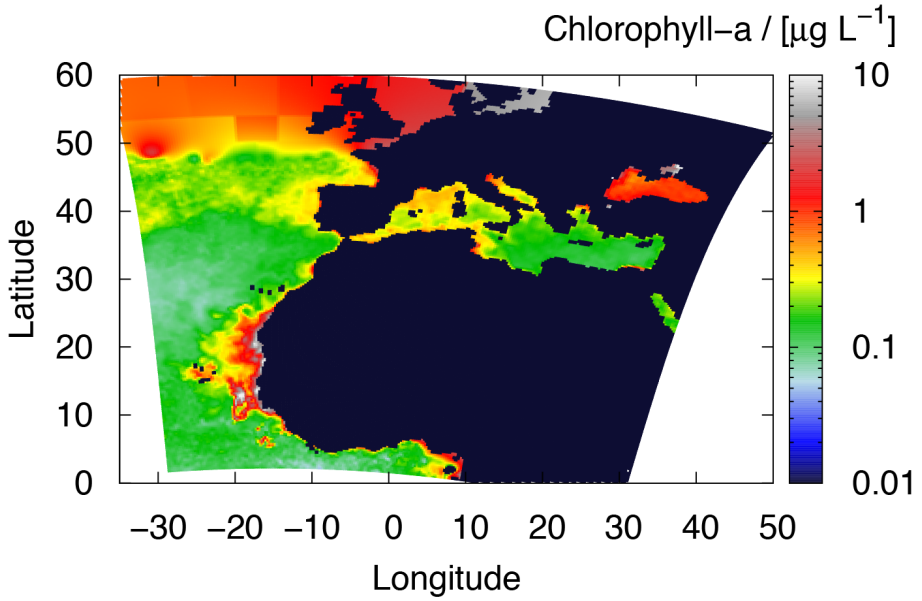


**Fig. 4.** Monthly averaged surface chlorophyll *a* concentration merged and interpolated from MODIS-AQUA and MODIS-TERRA data for December 2007.





ACPD
14, 377–434, 2014



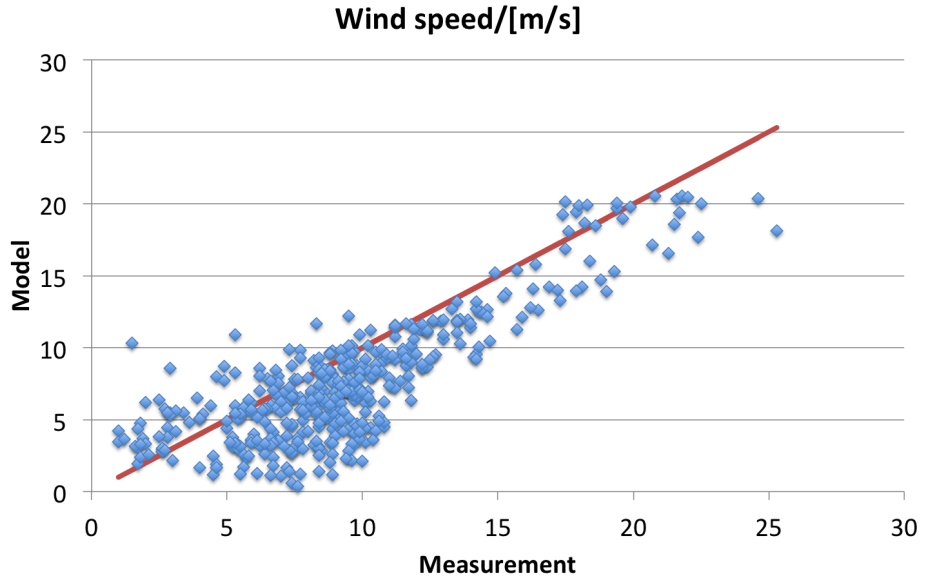


**Fig. 5.** Modelled first layer wind speed compared to measurements made during an Atlantic transsec (Cape Town towards Bremerhaven) with the research vessel *Polarstern* between 28 April 2011 and 17 May 2011 compared to the 1 : 1 line.





ACPD
14, 377–434, 2014



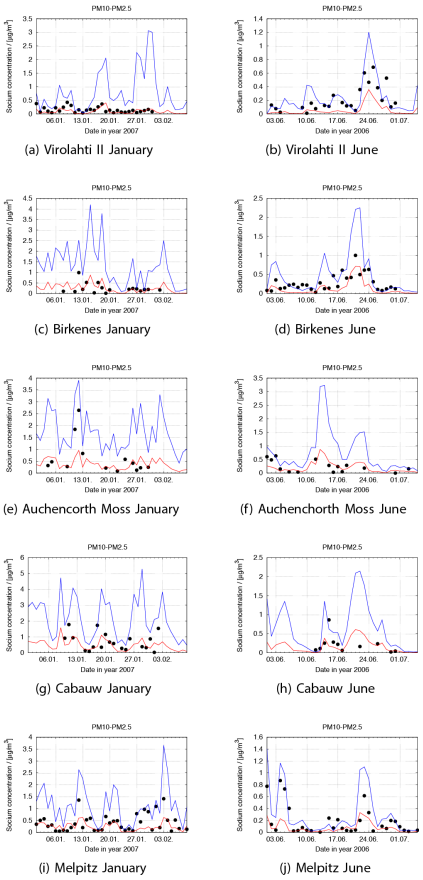


**Fig. 6.** Modelled $PM_{10}$–$PM_{2.5}$ sodium mass concentration without SST correction (blue lines) and with SST correction using S11 (red lines) compared to EMEP measurements (black symbols).





ACPD
14, 377–434, 2014



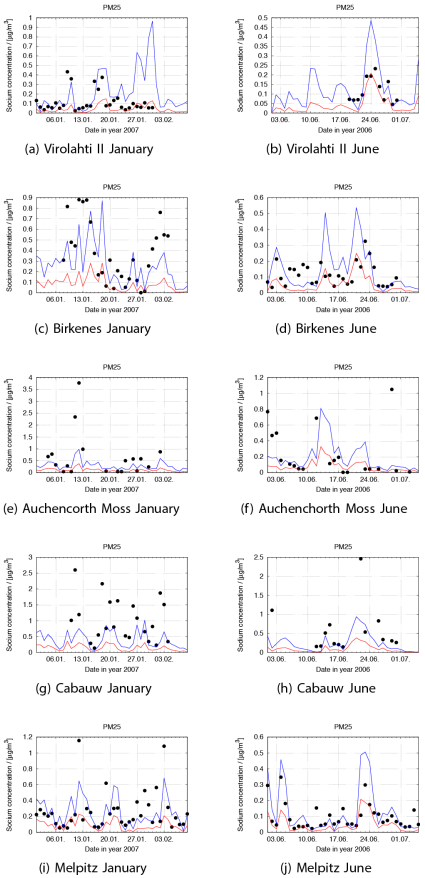


**Fig. 7.** Modelled $PM_{2.5}$ sodium mass concentration without SST correction (blue lines) and with SST correction using S11 (red lines) compared to EMEP measurements (black symbols).





ACPD
14, 377–434, 2014



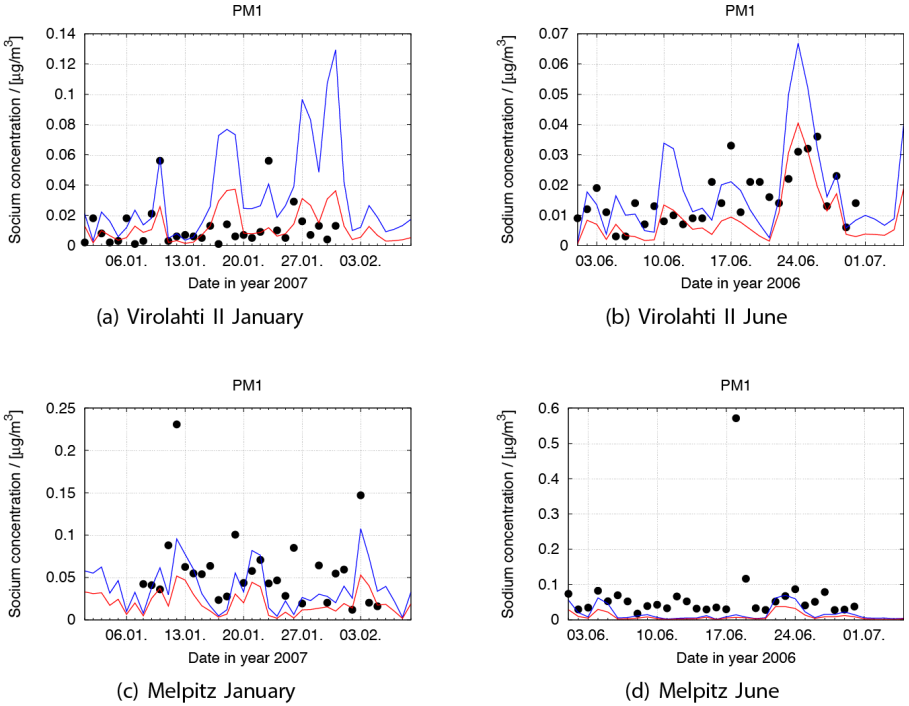


**Fig. 8.** Modelled $PM_1$ sodium mass concentration without SST correction (blue lines) and with SST correction using S11 (red lines) compared to EMEP measurements (black symbols).





ACPD
14, 377–434, 2014



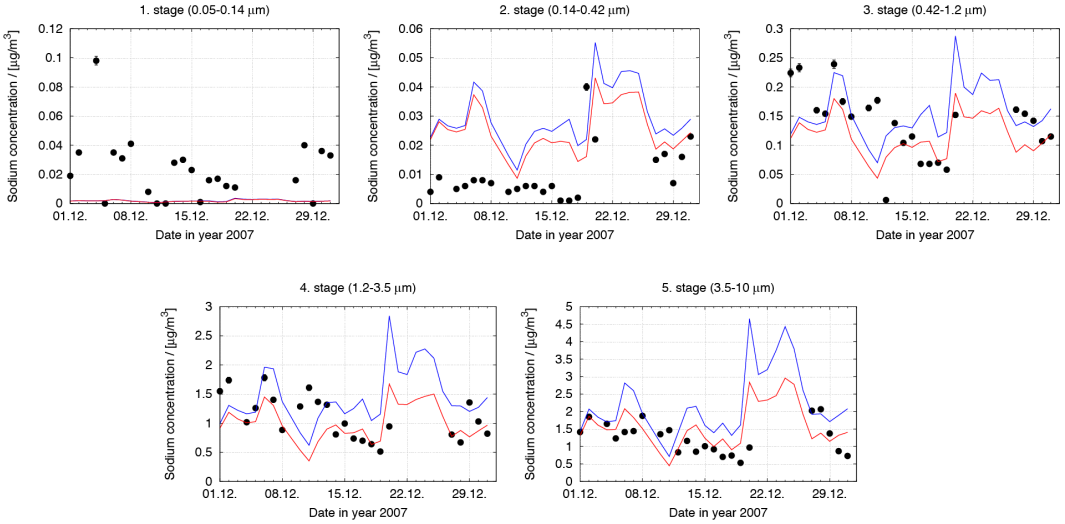


**Fig. 9.** Modelled sodium mass concentration without SST correction (blue lines) and with SST correction using S11 (red lines) compared to the Berner-impactor measurements at Sao Vincente (black symbols) for December 2007.





ACPD
14, 377–434, 2014



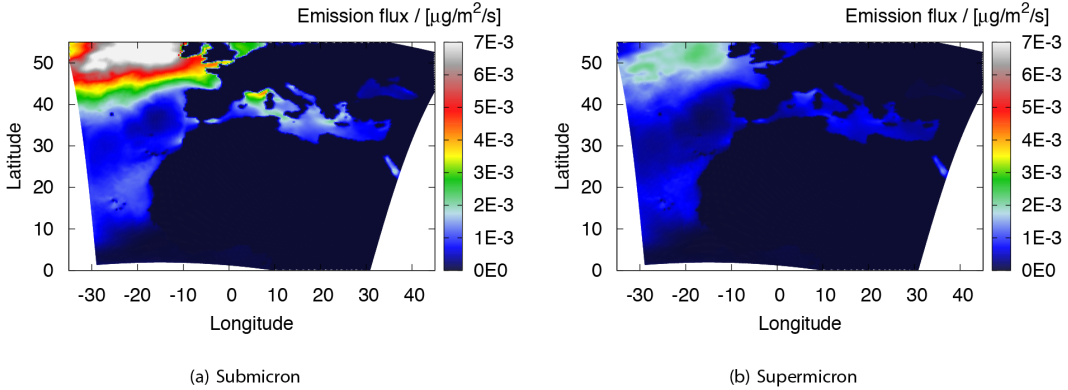


**Fig. 10.** Modelled monthly averaged emission fluxes of organic carbon for December 2007.





ACPD
14, 377–434, 2014



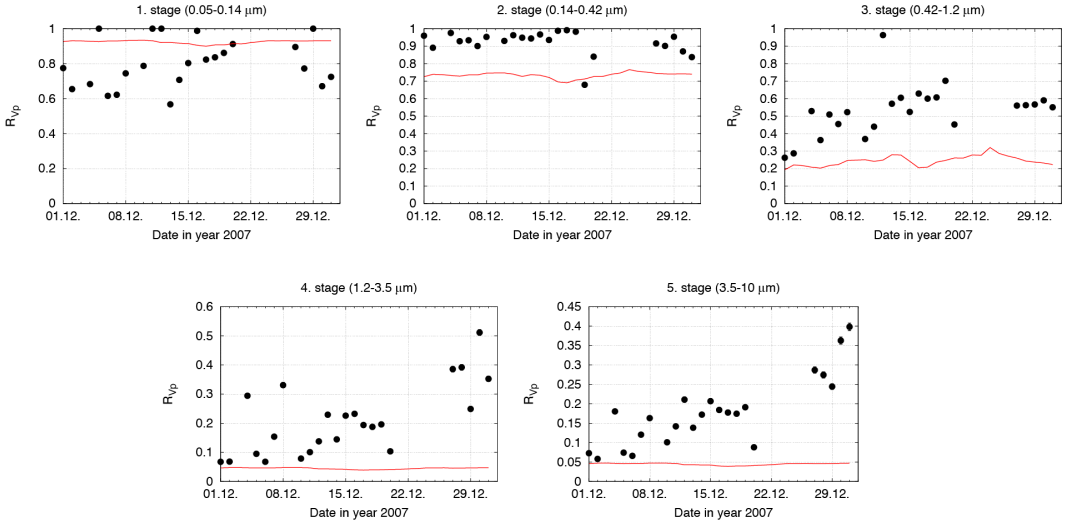


**Fig. 11.** Modelled $R_{Vp} = V_{OM}/V_p$ in the aerosol phase compared to measurements with a Berner-impactor at Sao Vincente (Cape Verde).





ACPD
14, 377–434, 2014



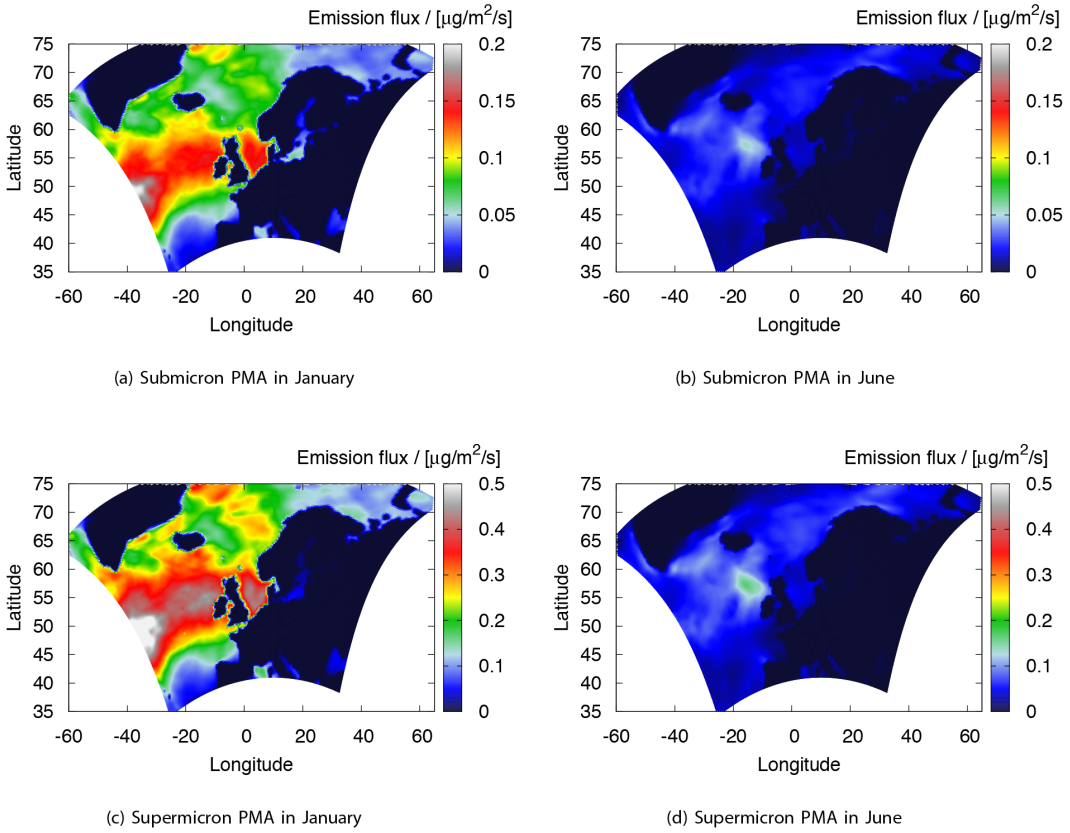


**Fig. 12.** Monthly averaged total PMA mass emission fluxes for submicron (top panels) and super micron (bottom panels) PMA emission in January 2007 (left panels) and June 2006 (right panels).





ACPD
14, 377–434, 2014



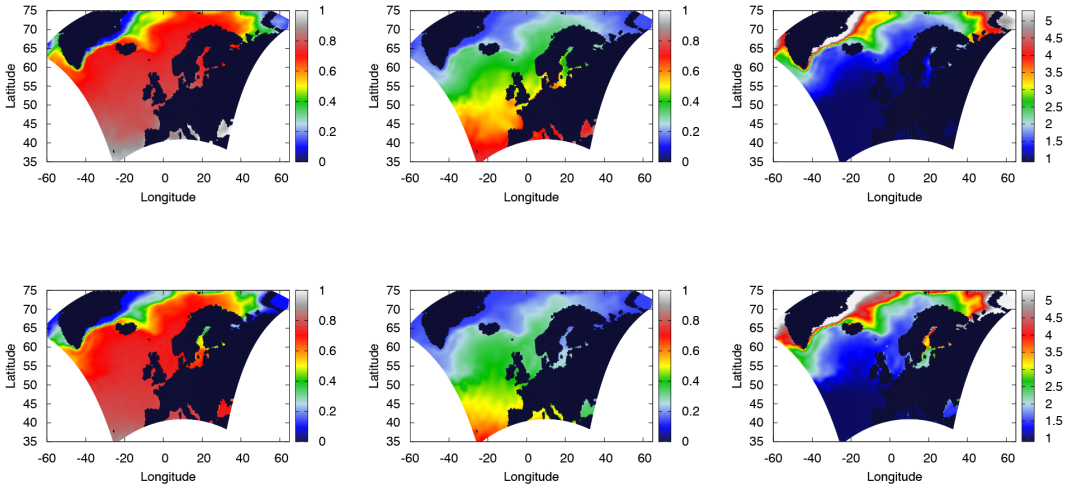


**Fig. 13.** Monthly averaged SST-correction factors for submicron PMA emission in June 2006 (top panels) and January 2007 (bottom panels) for the different parameterizations.





ACPD
14, 377–434, 2014



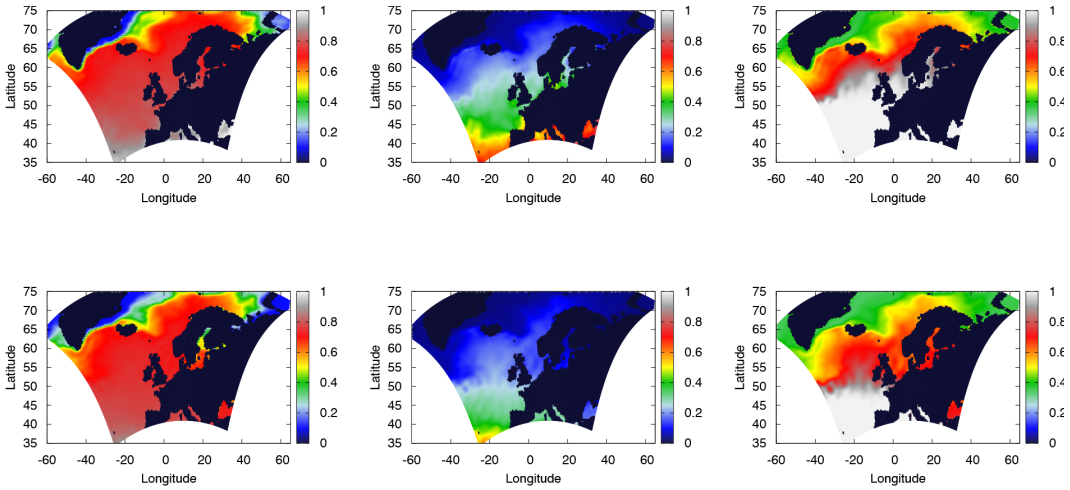


**Fig. 14.** Monthly averaged SST-correction factors for supermicron PMA emission in June 2006 (top panels) and January 2007 (bottom panels) for the different parameterizations.





ACPD
14, 377–434, 2014



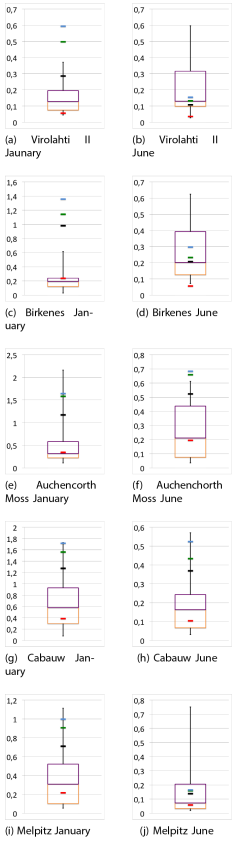


**Fig. 15.** Median of the sodium mass concentration in $PM_{10}$–$PM_{2.5}$ in $\mu g\,m^{-3}$ for S11 (red symbol), J11 (black symbol), Zb13 (green symbol) and no SST correction (blue symbol) compared to EMEP measurements.





ACPD
14, 377–434, 2014



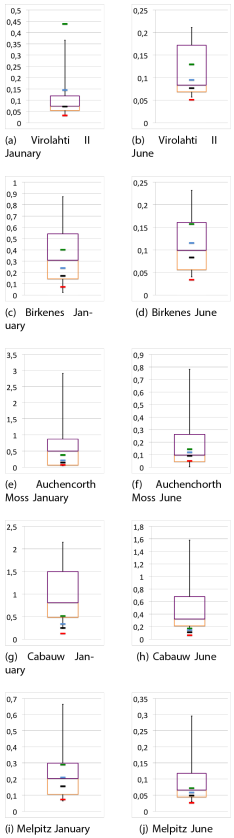


**Fig. 16.** Median of the sodium mass concentration in $PM_{2.5}$ in $\mu g\,m^{-3}$ for S11 (red symbol), J11 (black symbol), Zb13 (green symbol) and no SST correction (blue symbol) compared to EMEP measurements.





ACPD
14, 377–434, 2014



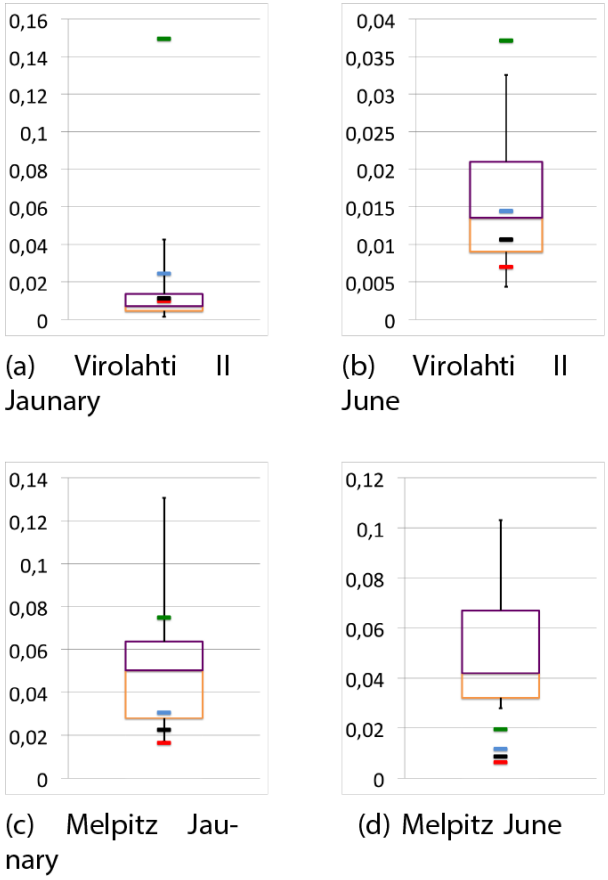


**Fig. 17.** Median of the sodium mass concentration in $PM_1$ in $\mu g\,m^{-3}$ for S11 (red symbol), J11 (black symbol), Zb13 (green symbol) and no SST correction (blue symbol) compared to EMEP measurements.





ACPD
14, 377–434, 2014



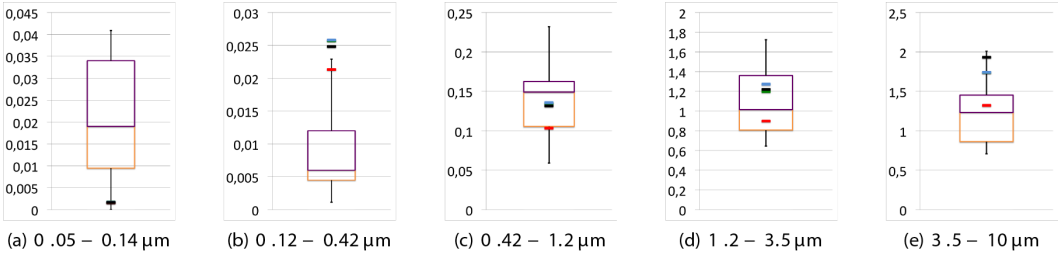


**Fig. 18.** Sodium mass concentration in $\mu g\,m^{-3}$ for S11 (red symbol), J11 (black symbol), Zb13 (green symbol) and no SST correction (blue symbol) compared to Berner-impactor measurements (Boxplot) at Sao Vincente.





ACPD
14, 377–434, 2014